

Channel Models and Beamforming at Millimeter-Wave Frequency Bands

Katsuyuki HANEDA^{†a)}, *Nonmember*

SUMMARY Millimeter-wave (mm-wave) radio is attracting attention as one of the key enabling physical layer technologies for the fifth-generation (5G) mobile access and backhaul. This paper aims at clarifying possible roles of mm-wave radio in the 5G development and performing a comprehensive literature survey on mm-wave radio channel modeling essential for the feasibility study. Emphasis in the literature survey is laid on grasping the typical behavior of mm-wave channels, identifying missing features in the presently available channel models for the design and evaluation of the mm-wave radio links within the 5G context, and exemplifying different channel modeling activities through analyses performed in the authors' group. As a key technological element of the mm-wave radios, reduced complexity beamforming is also addressed. Design criteria of the beamforming are developed based on the spatial multipath characteristics of measured indoor mm-wave channels.

key words: millimeter-wave, channel model, radio wave propagation, beamforming, antennas, fifth-generation, 5G

1. Introduction

High-data-rate wireless data transfer is one of the most essential needs of the modern society to get access to flood of information available anywhere at anytime. The wireless network infrastructure serving the backhaul and access links is facing challenges to cope with increasing mobile data traffic. Deployment of the fourth-generation cellular radio standards, the Long Term Evolution, and cellular offloading effort through wireless local area networks and device-to-device communications has been in progress. However, the drastic increase of the mobile data traffic will most likely exceed the capacity of the being-reinforced wireless network infrastructure soon. For this reason, the development of fifth-generation (5G) mobile networks has been the interest of operators and mobile device manufacturers. Collective actions towards the development have been initiated in different parts of the world. One of such actions is the European framework program 7 call 8 project METIS2020 [1], which aims at improved per-area spectrum efficiency, energy efficiency, and end-to-end latency. Among the candidate technologies in the physical layer that may lead to fulfilling the 5G target performance are the use of millimeter-wave (mm-wave) radio frequency spectrum and of a massive number of antenna arrays. Mm-wave radio frequencies have a number of distinct features that makes them attractive but also challenging for fulfilling the target. While abundant

radio spectrum available for communication worldwide is the most apparent reason to attract attention, the possibility of dense frequency reuse over spatial domain complements the global trend of moving towards small cells for efficient interference and energy management, leading to improved per-area spectral efficiency.

Deployment of mm-wave radios for broadband data transfer was considered in the late 80's for outdoor scenarios. The deployment mainly concerns fixed point-to-point links, where the radio wave propagation in urban street canyons and the attenuation due to penetration through tree canopies were reported already as influential phenomena of such links [2], [3]. Later in the 90's the deployment scenario was extended to indoor scenarios where human blockage and penetration loss through walls are the major interests of investigation to determine the coverage and the link budget. A large number of papers were produced for the indoor channel modeling and reporting the importance of interplay of propagation channels with directional antennas in terms of alignment and polarization [4]–[6]. The main research interests were link budget, delay dispersion, and Doppler effects. Later the use of slightly higher frequencies in the mm-wave band became an interest of the industry, which is facilitated by the orders of the FCC [7] and recommendation of the ECC within the CEPT [8] that define service rules for the spectrum use of 71–76 GHz, 81–86 GHz, and 92–95 GHz bands for fixed point-to-point wireless local area networks. The service is expected to use highly directional antennas not only for ensuring the quality of the intended link, but also for minimizing the interference to the other links operating in the same environment for coexistence. Directional communications are also specified as a means to extend the coverage in the standards for wireless personal and local area networks in small-area, i.e., the IEEE 802.15.3c-2009 [9] and 802.11ad-2012 [10]. The standards and following industrial activities have made various products available in consumer applications for wireless high-definition multimedia interface [11], [12]. Given the progress in complementary metal-oxide-semiconductor technology for manufacturing mm-wave radio frequency chipsets, the mm-wave radios can serve as a viable cost-effective solution to provide broadband data connection [13]. The mm-wave radios for the coming 5G backhaul and mobile may be defined as a convergence of outdoor and indoor mm-wave infrastructure and access schemes that are summarized above, and are characterized as

Manuscript received September 1, 2014.

Manuscript revised December 22, 2014.

[†]The author is with the Aalto University School of Electrical Engineering, Espoo, Finland.

a) E-mail: katsuyuki.haneda@aalto.fi

DOI: 10.1587/transcom.E98.B.755

1. Multi-user and multi-site access capability through intelligent management of interference and co-existence over space using beamforming;
2. Access points (or base stations) that can handle both small-cell short-range access links and medium-range wireless back- or front-haul links;
3. Support of moderate user mobility, and even dual-mobility in case of a device-to-device communication; and finally,
4. Coordinated operation of the network with lower microwave frequencies as a fall-back option.

There has already been several reports that discuss the feasibility of mm-wave mobile broadband access [14]–[16], which includes a demonstration of directional mobile access through beamforming. As one of the limiting factors of any radio system, radio wave propagation at the mm-wave band has already been an interest of those who design and evaluate the systems since the 80's. There have been significant effort devoted to the measurement and modeling of mm-wave radio channels. Since new requirements and functions of radio systems are emerging as summarized above, radio channel models need also refinement such that they are usable for the design and evaluation of the functions [17]. The main goal of this paper therefore is to provide a survey on the available channel models for mm-wave bands and discuss their possible improvement for the purpose of 5G-relevant mm-wave radio link design and evaluation. As a concrete example, stochastic and site-specific channel modeling activities of the authors' group are introduced. The present paper then gives a summary of beamforming schemes, which are essential functions for the mm-wave radios to be a strong candidate technology for 5G mobile network. Beamforming design criteria will be elaborated by the analysis of authors' group. The paper finally lists an essential but missing features of channel modeling that needs to be complemented by collective efforts of channel measurements and modeling.

This paper is organized in 6 sections. After this introduction, Sect. 2 summarizes generic features of a channel model that needs to be equipped for the purpose of radio link design and evaluation. Section 3 then introduces specific examples of available channel models following the classification into stochastic and site-specific models. Section 4 turns our attention to beamforming for mm-wave where the tradeoff between complexity and performance gains is of the utmost importance. Section 5 discusses challenges in establishing mm-wave channel models for fulfilling the 5G target performance and mentions possibilities to address the challenges. Section 6 concludes the paper.

2. The Radio and Propagation Channels

As a general framework of radio channel modeling, this section distinguishes the multipath propagation and radio channels to highlight their levels of abstraction for the channel modeling. Mathematical expressions of the radio and propa-

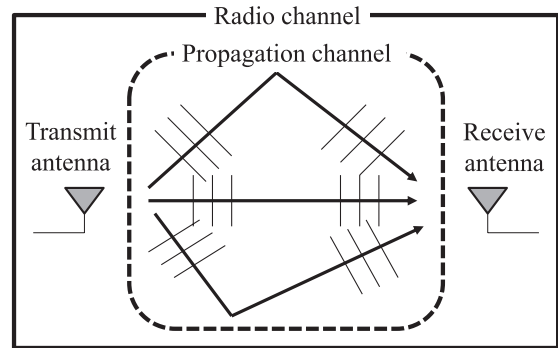


Fig. 1 The radio channel consists of the Tx antenna, multipath propagation channel, and the Rx antenna. The propagation channel is always given in the context of radio communication which we cannot engineer, while the Tx and Rx antennas are what we can engineer. The radio channel response includes characteristics of the Tx and Rx antennas and the propagation channel illuminated by the antennas [18].

gation channels are given, which are generic and applicable to both indoor and outdoor scenarios, and both to cellular and small-area coverage as far as far-field electromagnetic propagation is dominant.

The radio signals that transfer the data wirelessly over the physical environment go through three physical entities, i.e., transmit (Tx) antenna, multipath propagation, and receive (Rx) antenna. The multipath propagation is something we are always given in the context of radio communication and cannot engineer for performing better to improve the link. The propagation channel is independent of antennas, and the radio channel responses are determined once the Tx and Rx antennas illuminate the propagation channel. Figure 1 illustrates the decomposition of the radio channel into antennas and the propagation channel [18].

2.1 Multipath Propagation Channels

Looking at the propagation channel, the most popular way to express it is through a superposition of an infinite number of plane waves at a time instant t and a single frequency f , denoted as

$$\mathcal{P}_p = \left\{ \alpha_l, \mathbf{\Gamma}_l, \mathbf{\Gamma}'_l, \tau_l \right\}_{l=1}^{\infty}, \quad (1)$$

where $\alpha \in \mathbb{C}^{2 \times 2}$ is a polarimetric complex amplitude, $\mathbf{\Gamma} = [\phi \ \theta]$ and $\mathbf{\Gamma}' = [\phi' \ \theta']$ are vectors composed of azimuth and polar angles of the plane wave radiation and reception at the Tx and Rx, respectively, and τ is the propagation delay time. The polar angle θ is related to the elevation angle ψ as $\theta = \pi/2 - \psi$. A symbol with subscript $(\cdot)_l$ means a parameter value for the l -th plane wave, while the quantity represents the Rx side if a symbol is with a prime $(\cdot)'$. In practice, the number of plane waves is limited to L due to the limited dynamic range of the channel.

2.2 Radio Channels

A multiple-input multiple-output (MIMO) antenna channel

at a frequency f and a time instant t is expressed in an equivalent baseband form as

$$\mathbf{y} = \mathbf{H}\mathbf{x} + \boldsymbol{\xi}_n, \quad (2)$$

where $\mathbf{x} \in \mathbb{C}^N$ is an input signal vector to the Tx antenna ports, \mathbf{H} is a transfer function matrix of a MIMO radio channel, $\mathbf{y} \in \mathbb{C}^{N'}$ and $\boldsymbol{\xi}_n$ are the output signal and the complex white Gaussian noise vectors at the Rx antenna ports, respectively; N and N' denote the number of Tx and Rx antenna elements. The (j', j) -th entry of the MIMO channel matrix is a channel transfer function of the radio channel between the j -th Tx and j' -th Rx antenna elements, and is derived from the propagation channel (1) by combining the antenna far-field patterns as

$$h_{ij} = \sum_{l=1}^L \mathbf{g}_j^H(\boldsymbol{\Gamma}_l) \alpha_l \mathbf{g}_j(\boldsymbol{\Gamma}_l) \exp\{-j2\pi f \tau_l\} \quad (3)$$

where $\mathbf{g}(\boldsymbol{\Gamma}) \in \mathbb{C}^2$ is a polarimetric complex gain of the antenna element to the direction $\boldsymbol{\Gamma}$. The operation \cdot^H denotes the Hermitian transpose. The phase of the complex gain of the antenna elements are defined with respect to an origin of the coordinate system of the radio channel.

2.3 Characteristics Parameters of Radio Channels

The transfer function of the radio channel (3) is a basis for any channel modeling and hence different characteristics parameters of the channel can be extracted from it. For example, the small-scale fading is determined by a variation of its normalized magnitude, while the pathloss and shadowing are derived from the mean magnitude of them; the time-varying channel impulse responses and instantaneous Doppler spectrum is derived from the time-varying transfer function using the Fourier transform [19], [20]. Power delay profiles (PDPs) and the Doppler spectrum yields from an ensemble average of the instantaneous realizations. Their first- and second-order moments are the mean delay, delay spread, and Doppler spread [20]. Similarly it is straightforward to derive the Tx and Rx power angular spectrum (PAS) by applying the Fourier transform to the transfer functions across antenna array elements. The second order moment of the PAS is called the angular spread. As a relationship of the Fourier pair, the delay, Doppler, and angular spreads are inversely proportional to the channel coherence over the frequency, time, and distances [19], [20].

3. Survey on Mm-Wave Radio Channel Models

Channel models are tools to reproduce the physical parameters of the propagation channel (1), the transfer function of the radio channel (3), or their characteristics parameters summarized in Sect. 2.3, using mathematical expressions. The reproduced channels must resemble the measured ones and retain their characteristics parameters. Structure, accuracy, and the computational complexity of the model is

different for what to reproduce, i.e., the physical parameters, the transfer functions, or the characteristics parameters. The models for physical parameters (1) tend to have a complex structure, while they have flexibility in terms of antenna types at the Tx and Rx. The models for transfer functions (3) and characteristics parameters are always specific to certain antennas at the Tx and Rx. Since antenna reconfigurability due to, e.g., beamforming, is one of the most distinguished features and is playing an important role in the mm-wave radio links, the models for physical parameters have been found most versatile. This section summarizes available channel models for physical parameters, transfer functions, and characteristics parameters.

3.1 Stochastic Channel Models

Stochastic channel models reproduce the parameters of interest based on observation of measured channels and statistics of the characteristics parameters. This approach is considered as a generalization of measured channels and hence is often used as a reference channel model with which the performance of different physical layer schemes is analyzed and compared.

3.1.1 Large-Scale Models

Pathloss and shadowing: Most works reported in the literature discuss the large-scale and small-scale models separately. The most important large-scale characteristics parameters of the radio channel are pathloss and shadowing, which have been reported for a variety of indoor and outdoor environments both in line-of-sight (LOS) and non-LOS (NLOS) cases. It may not be straightforward to establish a pathloss model that is applicable for varying types of antennas since they illuminate propagation channels differently depending on their beamwidth and orientation. This is especially a critical issue at mm-waves where antennas are equipped with beamforming. Reported mm-wave pathloss models often include the effect of high directionality of antennas, leading to large shadow fading due to fluctuation of the received power for different antenna pointing angles, while there are models with omni-directional antennas that were either obtained from channel sounding campaigns with omni-directional antennas or synthesized from directional antenna measurements [21]. [22] provides a summary of pathloss exponents and shadowing reported in previous literatures for indoor environments. The summary proposes generic indoor and office pathloss models for LOS and NLOS cases. The summary furthermore concludes that there is no significant difference of the pathloss exponent between the use of omni-directional or directional antennas. For outdoor cellular scenarios, a seminal work [23] reports pathloss exponents of 3.6 and 10.4 for the intended- and outside-coverage areas at 55 GHz in urban microcellular street canyon scenarios. A number of pathloss exponents and shadowing estimates are reported [24]–[28] for a peer-to-peer and cellular outdoor scenarios at various mm-wave

Table 1 Summary of pathloss and shadowing parameters in indoor and outdoor scenarios. In case papers report multiple pathloss results from, e.g., different measurement sites, only representative values are shown for brevity.

Ref.	Scenario	Freq. [GHz]	Pathloss exp.		Shadowing [dB]	
			LOS	NLOS	LOS	NLOS
[22]	General indoor	60	1.7	3.3	1.8	4.6
[23]	Cellular	55	3.6		3.2	
[26]	Peer-to-peer	60	2.23	4.19	1.87	9.98
[27]	Peer-to-peer	60	2.25	4.22	2.0	10.12
[27]	Cellular	38	2.22	3.88	1.37	11.43
[27]	Peer-to-peer	38	2.0	4.57	3.79	11.72
[28]	Cellular	28	2	2.92	5.8	8.7
[28]	Cellular	73	2	2.45	5.8	8.0

frequencies as summarized in Table 1. Dependence of the base and mobile antenna heights on the pathloss exponent and shadowing values are reported in [29], [30]. A heuristic pathloss model for 28 GHz including the effect of shadowing due to buildings is introduced in [31].

Excess pathloss due to oxygen absorption, water vapor, rain, hail, and foliage are covered in [32]–[40], along with the recommendation of the International Telecommunication Union for predicting attenuation due to rain [41] and fog and cloud [42]. The losses due to various shadowing objects on a street such as pedestrians and cars at 60 GHz are summarized in [4]. Brick walls and tinted glasses which are most likely coated by metallic film incur more than 25 dB losses easily in penetration and hence are almost serving as isolating media [2], [43], [44]. [45], [46] report pathloss models at 60 GHz for inter-vehicular scenarios in various traffic conditions with link-shadowing cars in-between, showing the pathloss exponent being close to or smaller than the free space and the significant excess loss due to the link-shadowing cars. Human bodies are also relevant link shadowing objects both in the indoor and outdoor context. Experimental works of characterizing the human body shadowing in indoor scenarios show up to 20 dB excess losses [47], [48].

Shadow duration: The time period where the link shadowing persists affects the link outage performance significantly. Shadow duration due to human activities has been reported in various indoor environments. For example, temporal variations induced by the moving people leads up to 50 ms of coherence time of a radio channel at 60 GHz [49], and up to 3 ms at 30 GHz [50], [51]. On the other hand, [47] shows that the human body shadowing lasts for a median period of 100 ms in a scenario with one-to-five person walking and for 300 ms with 11-15 persons. A similar analysis for a crowded aircraft cabin [48] reports maximum and median depth durations of 8000 and 500 ms.

Delay spread: Delay spread is another important characteristics parameter that determines the intersymbol interference in single-carrier transmission and the frequency-flatness of the subcarriers in multi-carrier physical layer schemes [20]. It is reported in various literatures that directional antennas are effective in reducing the delay spread, along with the use of circular polarizations [52]–[55], though the effectiveness

Table 2 Summary of angular spreads reported in literatures, all reported at 60 GHz radio frequency. Unless explicitly stated, the dimensionless normalized angular spread is shown. If papers report multiple results from, e.g., different antenna locations, only a mean or indicative value is shown.

Ref.	Scenario	Angular spread values
[66]	Hallway	MS: 0.36–0.78
[66]	Room	MS: 0.62–0.84
[66]	Hallway-room	MS: 0.63–0.81
[67]	Office	MS: 0.4 (OLOS), 0.3 (NLOS)
[68]	Office	BS: 0.2 (LOS), 0.5 (OLOS), MS: 0.5 (LOS), 0.9 (OLOS)
[69]	Office	BS: 55.1° (azimuth), MS: 65.5° (azimuth), 16.5° (elevation)
[70]	Office	BS: 19° (azimuth), 18° (elevation)

of the latter is channel-dependent [56]. Devising a generic model of delay spread for varying types of antennas and environments is a difficult task at mm-waves because of its huge variation depending on the beamwidth and orientation of the Tx and Rx antennas. The seminal work [57] reports the delay spread up to 200 ns in an outdoor setting, while several papers report delay spreads lower than 20 ns in the best cases, even with NLOS outdoor scenarios, e.g., [26], [58]–[60]. A summary of delay spread values reported in major literatures with varying antenna configurations in indoor scenarios is available in [61]. [62]–[64] reports the delay spread under the presence and absence of human bodies in in-vehicle and aircraft cabins. [65] infers a proportionality of the delay spread with the size of the room.

Angular spread: Angular spread represents the multipath richness seen at the antennas that determines the effectiveness of the spatial and angular diversity and spatial multiplexing. The reported angular spread values [66]–[69] are mostly for indoor scenarios as summarized in Table 2. The normalized angular spread is a dimensionless quantity and ranges from 0 to 1, corresponding to highly angularly selective and dispersive channels, respectively [66]. The maximum angular spread is observed in a uniform power spectrum that yields azimuth and elevation angular spread in degree of 104° and 52°. [70] reports angular spreads of an indoor NLOS channel for different Tx and Rx antenna polarizations, showing that they vary about $\pm 40\%$ and $\pm 10\%$ around the median value on the azimuth and elevation domains, respectively. The angular spread values in outdoor cellular scenarios are presently lacking, though there have been several measurements that allow for them, e.g., [24], [28], [71].

3.1.2 Small-Scale Models

Power spectrum models: The widely-used approach of small-scale channel modeling is characterization of the shape of PDP, PAS, and the Doppler spectrum. The spectrum shape allows us to reproduce physical parameters (1) in a statistical manner. The spectrum shape is determined solely by observation of the measured channels as summarized in the following.

Power delay profiles: The popularly observed shape of the

PDP in measurements is a single or superposition of multiple exponentially decaying spectrum. Each of the exponentially decaying spectrum is treated as a unit to build the entire channel and called a cluster [72], [73]. The PDP shape has been reported in the microwave frequency band originally, and the same shape was also found applicable at the mm-wave band [74]–[76]. A simplified shape model yields the tapped delay line model, e.g., as reported for indoor rooms [77] at 62 GHz and outdoor fixed links [33], [78] around 30 GHz. The delay-domain multi-cluster model is parameterized in various scenarios, such as desktop [79], residential, office, and kiosk [80], cubicle office [81], [82], a conference room [83], and inside a passenger car compartment [84]. A number of refinement is made compared to the original multi-cluster model; the desktop model [79] introduces a two-path model in addition to the multi-cluster model that represents the fading due to LOS and a reflection from a desk. The conference room model [82] introduces an exponential power decay of clusters over delay *before* the cluster peak, in addition to those after the peak. They are called pre-cursor and post-cursor intra-cluster models, which are observed often when the main beams of antennas are pointing to one of the scattering objects in a cluster. These extensive works constitute the standardized indoor channel models for the IEEE 802.15.3c [85] and the 802.11ad [86] task groups. Further extension of the model is performed, for example, towards a unified delay domain small-scale channel model that is applicable for microwave and mm-wave ultrawideband channels [87]. [88] complements the cluster parameters following the principle of the 11ad-model, and furthermore found that small fixtures such as ceiling lamps and shelves are often visible as clusters, despite they are neglected for the sake of simplicity in the 11ad-model. As an alternative model, the papers [89], [90] characterize their measured PDPs as a combination of specular and diffuse components that appear as discrete spikes and continuously decaying power spectrum over delay, respectively. The diffuse spectrum behaves as if it was a noise floor, as commonly observed in PDPs at microwave frequencies [91]. An exemplary PDP measured at 60 GHz in a large indoor scenario is depicted in Fig. 2, where the diffuse spectrum is clearly visible but occupies only 10% of the total received power [92].

Power angular spectrum: Various channel sounding reveals that a PAS at mm-wave is typically modeled as superposition of clusters as commonly reported in microwave frequency channels, e.g., [73]. In particular, [88], [93] report Laplacian distribution cluster PAS with the standard deviation of 15° in indoor channels. [79] reports the standard deviation of 35° in desktop scenarios. The works [24], [28], [60], [94] report an angularly-selective PAS in built-up urban areas at 28 and 73 GHz. In [24], [28], maximum 4 main directions of multipaths were observed at an elevated base station and a mobile, with each direction having angular spreads of about 15° and less than 6° in azimuth and elevation, respectively. The works [60], [94] on the other hand report a larger number of directions available in similar

dense urban environments, with no information of the angular spread. The indoor channel sounding [70] shows clear clustering of multipaths according to the PAS and power angular-delay profiles. In contrast, there are also works reporting PAS spread over wide angular range; [71] shows PAS of outdoor rooftop-to-ground channels at 28 GHz, revealing rich scattering even in LOS cases. The work [90] reports that radio channels in large indoor scenarios at 60 and 70 GHz show a uniform distribution of propagation paths over the azimuth angle, and that the path clustering phenomenon is not prevailing over the spatio-temporal domain. In the standard channel models for short-range scenarios [85], [86], the PAS is modeled as a set of clusters each having Gaussian or Laplacian distributed intra-cluster PAS. Their standard deviation differs significantly from 5° to over 100° indicating a very wide angular dispersion, depending on the scenario.

Doppler spectrum: The Doppler spectrum of the channel determines the average frequency-shift due to the movement of mobiles and changes in environments. Previous reports characterize time variation of the channel due to human activity mainly through the coherence time rather than the Doppler spectrum since it is possible at the mm-wave band to have large frequency spacing between two neighboring frequency tones that makes the Doppler-shift marginal. On the other hand, the maximum Doppler shift is intuitively higher at the mm-wave than at microwave frequencies due to the shorter wavelength [95], which can make the channel estimation quickly obsolete in case of a device mobility. The Doppler power spectrum in an indoor scenario is reported to have a Laplacian shape centered at 0 Hz along with peaks due to florescent lights at 50 and 100 Hz [49], similarly to the previously reported indoor channel model [96]. In contrast, the Doppler spectrum of a cellular mobile channel has not been reported from measurements in literatures, partly because of high time sampling rate required.

Depolarization: Exploitation of orthogonal polarizations is an effective method to acquire extra degrees-of-freedom in radio channels and hence to increase the channel capacity while maintaining the form factor of the antenna array. Depolarization of transmitted electric fields during radio propagation is an important phenomenon that characterizes the cross-talk between two orthogonal polarizations and determines the extent of capacity gain. Only a handful of papers report the depolarization effects through the cross-polarization ratio (XPR) of propagation paths; [97] mentions a median XPR of 20 dB in large indoor channels at 70 GHz, while a contribution in [98] reports mean XPR values of 17.1 and 8.3 dB for specular and diffuse propagation in indoor 60 GHz channels. The high XPR values than those at microwave frequency bands manifest more effective increase of the capacity gain. Such analysis lacks in outdoor cellular environments presently.

Geometry-based models: A geometry-based stochastic channel model (GSCM) is another convenient way to reproduce the physical parameters of plane waves (1). Different from parameterizing the shape of power spectrum,

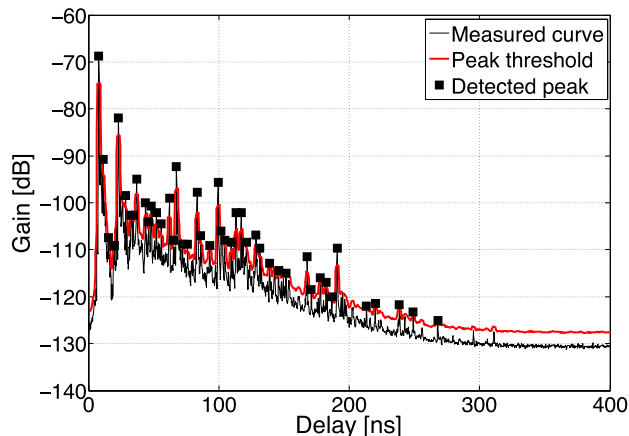


Fig. 2 An exemplary PDP measured in a shopping mall at 60 GHz. Reproduced from [90].

this model further elaborates attributes of multipath plane waves to physical but imaginary distribution of electromagnetic field scatterers. Creation of the scatterer distribution is made either on an imaginary map, e.g., [99], where each scatterer is characterized by the three-dimensional coordinate, or with angles of departure and arrival and delay of each scatterer seen from the Tx and Rx antennas, e.g., [100]. These approaches have similarities to the site-specific modeling detailed in Sect. 3.2 but are much simpler in mathematical characterization and computational load due to the assumption that the GSCM is based on an imaginary scenario. The GSCMs gain popularity in modeling the channels at the microwave frequencies and are used as a reference channel model for example in 3GPP [101] and ITU [102] thanks to their reasonable compromise between the accuracy and complexity. Selection of parameters in GSCM is an important design aspect to make the model output as realistic as measured channels in terms of the characteristics parameters defined in Sect. 2.3.

It is more straightforward to identify electromagnetic field scatterers in outdoor than indoor scenarios due to the existence of distinct objects that produce multipaths, such as walls of large buildings and high-elevated landmarks such as a tall tower [103]. The GSCMs at mm-waves therefore have been built for outdoor scenarios, a seminal work being for fixed point-to-point wireless links at 20 GHz [104]–[106]. Geometrical properties of wave scattering objects such as a height distribution of rooftops, tilt and orientation of building surfaces and their reflectivity are determined statistically. A GSCM for a fixed point-to-point link in suburban scenarios was proposed in [36]. More recently, the papers [107], [108] provides parameterization of electromagnetic field scatterer locations for a GSCM covering 81–86 GHz mm-wave band in a street canyon scenario. The scatterer distribution of the model [108] is presented in Fig. 3(a). The two dashed lines correspond to the line of building walls and the scatterers can exist both on the street and inside a building. The scatterers on the street possibly represent cars, foliage scattering, and lampposts, while those inside the build-

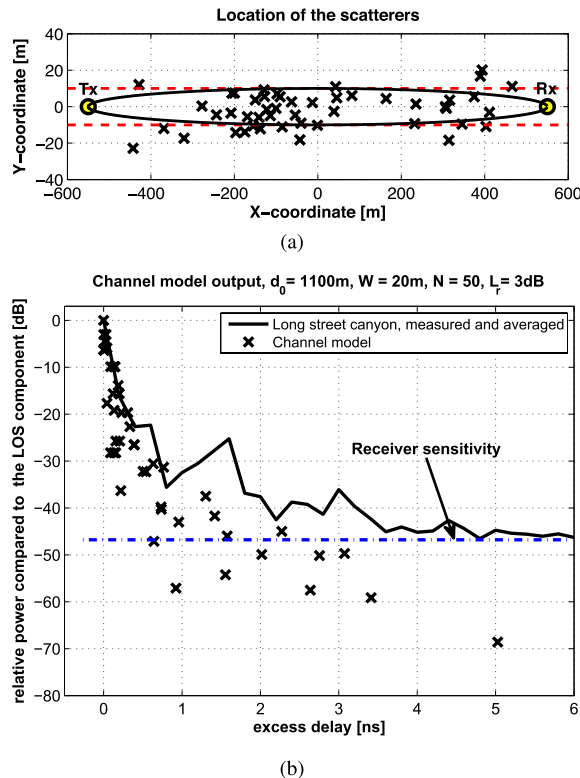


Fig. 3 Exemplary mm-wave GSCM for an outdoor street-canyon scenario at 81–86 GHz band. (a) The scatterer distribution and (b) the comparison of the reproduced multipaths and measurements. Reproduced from [108].

ing are allowed to consider multiple reflections from the building walls. The model output is compared with measured channels using the PDPs in order to demonstrate validity of the model as shown in Fig. 3(b). It is worth noting that the GSCM is not limited only to outdoor, but is also applicable to indoor scenarios. A part of necessary model parameters of the GSCM for outdoor channels at 28 and 73 GHz are presented in [28], [109], while those for indoor 60 GHz channels is reported in [110].

As in the street-canyon scenario, the scatterer distribution in the GSCM can reflect a specific layout of physical scatterers that characterize the propagation channel. An example is found in the mm-wave GSCM for inter-vehicular links [46], where the body and roof of a link-shadowing car and the ground are identified as major scattering points when simulating a channel between two vehicles. The car shape is simplified and modeled for the ease of determining the scattering points. Using the uniform theory of diffraction to calculate the diffraction losses, the model provides good agreement of pathloss in comparison with measurements. The works [111]–[113] allow over-the-rooftop propagation modeling by characterizing buildings as rectangular and cylindrical obstacles. A hybrid uniform theory of diffraction-physical optics approach is derived for accurate prediction of the pathloss in the vertically and horizontally polarized fields.

3.2 Site-Specific Models

Stochastic models that we have been reviewing so far are intended for design, evaluation, and comparison of different physical layer schemes. The stochastic models are therefore designed to be generic and minimize the specificity of the channels, such as measurement sites and antenna locations, and classify the channels only in an abstract level, such as outdoor/indoor and LOS/NLOS conditions. Considering the fact that there are plenty of different PDP shapes that lead to the same delay spread, the stochastic treatment of the channel through its moment values allows to generalize the channel model. The site-specific models, in contrast, aims at reproducing the channels at an intended location accurately for the purpose of coverage design for example. Recently the site-specific model is also seen as an alternative to channel sounding, provided that it is ensured that the model produces realistic channels well. It is advantageous to use the site-specific modeling along with measurements since the model can interpolate and even extrapolate the time-consuming and hardware-extensive channel sounding. In parameterizing the IEEE 802.11ad channel model, the joint use of channel sounding and site-specific model was promoted as an efficient approach [86].

3.2.1 Interaction between Waves and Objects

Site-specific models are implemented by ray- or geometrical-optics approximation of electromagnetic field propagation. The high radio frequency at the mm-wave band makes the approximation more suitable than the microwave frequency band. The sharp spatial transition in diffraction from the lit to shadowed regions suggests that the diffraction plays marginal role in wave propagation [114], [115]. There is a wide variety of material property characterization reported in the literature such as refractive index, relative dielectric parameters, reflection coefficients, and transmission losses per unit thickness [54], [116]–[130], along with the material parameters recommended by the ITU-R [131]. Different per-path human body shadowing models are proposed; for example, [132] uses a cylindrical metallic object as a model of a human body, showing that the shadowing depth does not change much for 2.4, 5.7, and 62 GHz in an indoor wireless link. [133] proposes to describe the human body as two intersecting metallic plates. They shadow the path of interest and produce diffracted paths from the two side edges and the top edge, and show close resemblance to measurements in terms of shadowing depth and duration. Along with those knowledge of wave interaction with objects, it is possible to predict the multipath propagation channel in a deterministic way.

3.2.2 Site-Specific Prediction Methods

Seminal works of site-specific channel prediction uses the

geometrical optics to analyze urban street-canyon scenarios and compares the results with measurements, showing sufficient agreement of delay spread [134]. Similar comparison between the prediction and measurements was performed also in various indoor and outdoor scenarios using received field strength distributions [135]–[139], delay spreads [140], [141], and PAS [142], [143]. There are different statements on the required order of reflection, diffraction and scattering for accurate prediction of PDPs; [144] shows that the fourth and sixth order reflections are required to predict small- and medium-sized rooms accurately in terms of the delay spread, while [139] considers first order reflection and diffraction, and foliage loss in outdoor settings, giving reasonable agreement of the received power at 12.5 and 30 GHz. Finally, a recent work [145] indicates that the first-order scattering may be enough. Different analyses of mm-wave channels [43], [146] show that the direct wave and the first-order reflected waves carries most power in LOS propagation environments, while diffraction and second-order reflection play an important role in NLOS propagation. The work [147] demonstrates agreement of channels inside a sport pavilion based on ray-tracing and measurements with varying complexity of building data, showing that the most complex building data would be needed to predict channels from inside to outside of the pavilion. The work [148] introduces a beam-tracing method instead of the ray-tracing to reduce the number of path traces in the prediction. It is often reported that the predicted and measured PAS and PDP show differences [149]–[151], which in many cases are attributed to the lack of diffuse scattering in the ordinal ray-tracing [69].

3.2.3 Scattering

Inclusion of the diffuse scattering is one of the necessary improvements of the site-specific channel modeling. Though the diffuse scattering is popularly reported at the microwave frequencies, e.g., [91], where the roughness of the scatterers are comparable to the wavelength, there is no consensus if the scattering is more dominant at the mm-wave or not since there are plenty of physical objects whose roughness is on the order of millimeter, e.g., brick walls [127] and small items on a desktop [71]. Scattering at mm-wave band has been reported in [152] through reflection coefficient measurements on cement walls with different surface roughness profiles at 28 and 38 GHz. The work concludes that the horizontal polarization is more sensitive to the roughness profile than the vertical polarization. [153] reports that diffuse scattering of electromagnetic fields is more dominant on a limestone wall than a brick wall at 28 GHz. The roughness also affects the diffracted fields e.g., behind a corner of a brick wall [127]. The use of the Kirchhoff Approximation [154] and the physical optics [155] are reported to estimate the wave scattering from rough surfaces well.

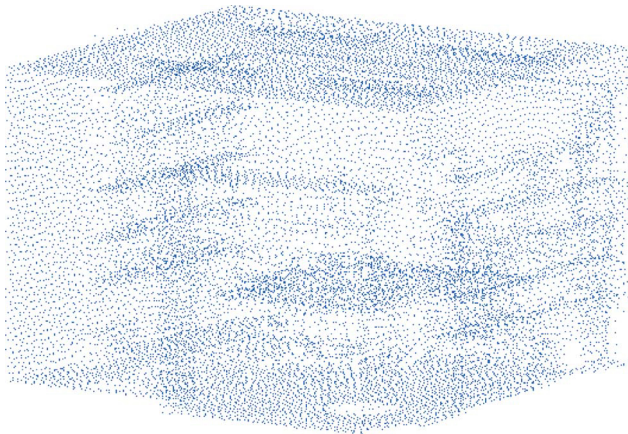


Fig. 4 Point cloud of a single room, reproduced from [145].

3.2.4 Field Prediction Based on Full-Scattering Approach

Site-specific field prediction based on full-scattering approach has gained little attention so far, but has more relevance at the mm-wave range due to the possible significance of physical objects that could have been insignificant at the microwave frequency range in terms of scattering. A seminal work [156] applies an elliptic scatterer distribution to site-specific indoor channel prediction. Received power of a single delay bin in a channel impulse response is a sum of multipaths originated from active scatterers on the ellipsoid. When the ellipsoid intersects a boundary of the environment, the intersection becomes active and produces scattered fields. A model in the infrared region is adopted to calculate the scattered field.

The works [145], [157], [158] use a fully-scattering approach to predict radio channels. The approach is based on an accurate structural data of the environment obtained from laser scanning; an example of the structural data is shown in Fig. 4. The scanner emits laser beams to many different directions to estimate spatial points from which the beams are bounced back using the two-way runtime measurements. The accuracy of the point measurements is usually on the order of or less than one millimeter. Aggregation of the points constitutes the structure of the environment called a point cloud. The use of the point cloud for site-specific field prediction is a new challenge, since the ordinal ray-tracing is not applicable directly and moreover obtaining a surface model of the environment from the point cloud is not necessarily an obvious task. When the separation between neighboring points in the point cloud is less than half-the-wavelength of the radio frequency, i.e., the Nyquist spatial sampling, the physical optics is applicable to yield rigorous solution of the scattered field. On the other hand, it is tempting to reduce the density of the point cloud so that the amount of scattering we calculate is smaller. To this end, the works apply the stochastic scattering model from a building wall proposed in [159] to the point cloud which does not necessarily fulfill the Nyquist

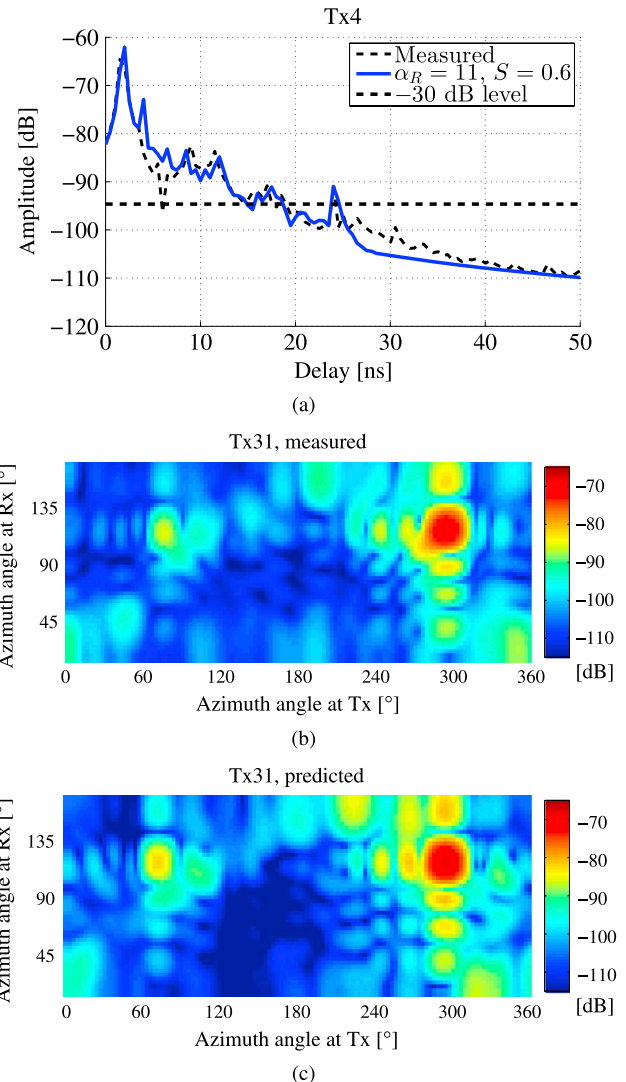


Fig. 5 Comparison of point-cloud-based field prediction and measurements: (a) PDP, (b) measured PAS, and (c) predicted PAS. Reproduced from [145].

spatial sampling. Different from the physical optics that assume omni-directional re-radiation from scattering objects, the stochastic scattering model can consider directional re-radiation due to the sub-Nyquist sampling. Comparison of the predicted and measured PDPs and PASs are shown in Fig. 5, demonstrating that the method can predict various types of channels dominated by diffuse scattering or specular reflections [158]. Main advantage of the method is that the surface roughness effect on the scattering is implicitly taken into account by means of the point cloud structural data of the environment, while the missing details of the material properties are complemented by the stochastic scattering model. Furthermore, it is not necessary to estimate the material characteristics of each point since they are holistically considered as *reflection coefficients of an environment* in the scattering model. The downside is that the stochastic scattering model always requires a calibration measurement

to obtain the reflection coefficients and the directivity of the scattering model. Practical feasibility in computation is another problem; even though the method requires much less computational load than the physical optics, the number of scattering waves is proportional to the number of points in the point cloud, making it difficult to apply to very large scenarios where millions of points may be required even with the sub-Nyquist spatial sampling of the environment.

4. Mm-Wave Beamforming

Since mm-wave radio frequency easily makes a physically small antenna aperture electrically large, mm-wave radios are inherently much more capable of focusing beams and obtaining gains through antenna aperture than at microwave radios. The beamforming capability is at the same time a required feature for mm-wave radios in order to compensate for the high losses of radio propagation and the human blockage [160]–[163]. What makes the beamforming more relevant for future cellular applications is its potential for dense spatial frequency reuse; pointing a narrow, so-called pencil beams towards the intended user keeps interference to other users minimal, making multiple concurrent wireless data transfers feasible in a confined area [164], [165]. Furthermore, having electrically large antenna arrays at the Tx and Rx allows spatial multiplexing; not only in multipath channels, but also in LOS-only channels where the antenna arrays create multiple pencil beams that illuminate different parts of the antenna aperture on the other side [166]–[168]. When analyzing the multipath effects on beamforming performance, it is necessary to be aware of the interplay between the antennas and radio propagation since it determines the degree of channel capacity improvement through gain focusing and spatial eigenmode transmission [169], [170]. Hybrid analog-digital beamforming is considered as an attractive solution when it comes to tradeoff between hardware complexity and channel capacity [16], [171]–[174], for which the interplay gives a number of design criteria of the beamforming. This section addresses these design and performance evaluation aspects of mm-wave beamforming in the context of spatial propagation channels at the mm-wave band, which are often reported to be more directionally selective than at the microwave band e.g., [24], [43], [68], [175]. For this purpose, we first elaborate the expression of a propagation channel defined in Sect. 2.1 to estimate the spatial degrees-of-freedom (SDoF) and the channel capacity of pencil- and eigen-beamforming. Based on these metrics, we then discuss design criteria and the capacity gain of the analog-digital beamforming using our exemplary measurement result in an indoor office room.

4.1 Eigenmode Transmission at Mm-Wave

The propagation channel is expressed as a set of physical parameters in (1) using an infinite number of plane waves. It is also possible to express the propagation channel in a form of a matrix \mathbf{M} , where the (j', j) -th entry $M_{j', j}$ represents the

transfer function between the j -th Tx *mode* to the j' -th Rx *mode* as [176]

$$\mathbf{M} = \sum_{l=1}^L \mathbf{F}'(\mathbf{\Gamma}'_l) \alpha_l \mathbf{F}^T(\mathbf{\Gamma}_l), \quad (4)$$

where $\mathbf{F}(\mathbf{\Gamma}) \in \mathbb{C}^{J \times 2}$ and $\mathbf{F}'(\mathbf{\Gamma}') \in \mathbb{C}^{J' \times 2}$ denote far-field electric field intensities of the modes at the Tx and Rx, respectively. The modes are orthonormal to each other, and in the three-dimensional free space they are expressed as spherical harmonics [177]. We remark the similarity of (3) and (4) but the functions \mathbf{F} and \mathbf{F}' representing the modes on the Tx and Rx sides respectively in (4) are *not* antenna radiation patterns, but are operators of the spherical Fourier transform to convert from the plane to the spherical wave domains. The dimension of the matrix \mathbf{M} is determined by the Tx and Rx antenna aperture sizes because of their mode truncation properties [177]. The underlying physics behind the truncation is that an electromagnetic field described by a mode index higher than J attenuates rapidly as it radiates from an antenna and does not propagate over space. A rule of thumb of the truncation is that the cut-off mode index is proportional to a minimum radius enclosing the whole volume of the antenna. This means that the use of a larger antenna aperture leads to a larger dimension of \mathbf{M} . The SDoF of the radio channel D_s is given by the rank of \mathbf{M} , and is an upper bound of the number of eigenchannels of any radio channels realized by antenna elements on the aperture [170], i.e.,

$$\text{rank}(\mathbf{H}) \leq \text{rank}(\mathbf{M}) = D_s, \quad (5)$$

where the equality holds only if the antenna elements exploit the available multipaths in the propagation environment properly. Larger antenna apertures give more SDoF if propagation channel conditions are favorable. Figure 6(a) shows the number of normalized eigenvalues of \mathbf{M} that exceeds different threshold levels $-t$ dB, meaning the estimates of the rank of the propagation channels at Rx signal-to-noise ratio (SNR) t dB. The normalization is performed with respect to the strongest eigenvalue. For the LOS case, the SDoF saturates around the antenna aperture size of $2\lambda^2$, while the SDoF of the NLOS case does not show the saturation until the antenna aperture size of $9\lambda^2$ because of the presence of more multipaths. The step increase of the curves is attributed to the floor function of the spherical harmonics truncation.

The channel capacity can be derived for the propagation channel matrix \mathbf{M} , similarly to the transfer function channel matrix \mathbf{H} . The capacity derived from \mathbf{M} is called an intrinsic capacity that can be realized by ideal lossless antenna apertures [178]. Similarly to the SDoF, the intrinsic capacity does not depend on the particular realization of antenna elements on the aperture, and can be derived by performing the water-filling power allocation to the eigenchannels of the propagation channel \mathbf{M} . Figure 6(b) shows the intrinsic capacity for channels with different Tx-Rx distances in an indoor LOS scenario [179]. The channel

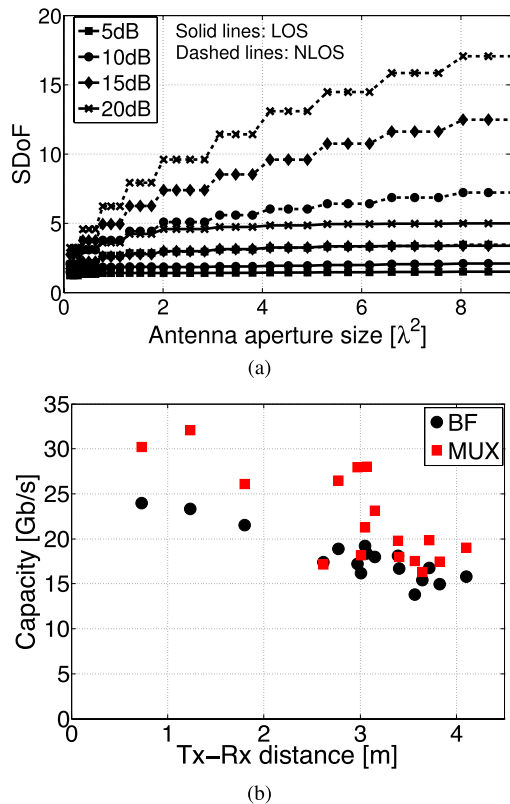


Fig. 6 (a) Variation of the SDoF on antenna aperture size. The SDoF is defined for different threshold levels, i.e., 5, 10, 15, and 20 dB. (b) Comparison of the Ergodic channel capacity when using the pencil- and eigen-beamforming, which are shown in BF and MUX labels respectively. The capacity values are derived from indoor mm-wave channels with 2 GHz bandwidth and -10 dBm Tx power, reproduced from [179].

capacity with pencil-beamforming is overlaid; the pencil-beamforming focuses the main beam to the direction of the LOS and hence no capacity gains are obtained through spatial eigenmodes. Antenna aperture size of the Tx and Rx is $9\lambda^2$. The pencil-beamforming gives lower capacity than the intrinsic capacity when the Tx-Rx distance is less than 3 m where the Rx SNR is high enough to exploit multiple SDoF of the channel in the case of eigen-beamforming. In contrast, the pencil-beamforming nears the intrinsic channel capacity when the Tx-Rx distance is beyond 3 m due to a small number of usable SDoF under the limited Rx SNR.

4.2 Hybrid Analog-Digital Beamforming

The SDoF and the comparison of the capacity between the eigen- and pencil-beamforming discussed in Sect. 4.1 serves as a number of design criteria for the beamforming in general. In mm-wave beamforming, the radio frequency chain is still costly and hence practically implementable beamforming architectures have been discussed. Antenna beamforming at mm-wave bands has mostly been relying on analog phase shifters, e.g., [162] for gain focusing, while the use of a few radio frequency chains for baseband digital beamforming leverages both the array and multiplexing

gain [95]. A hybrid of analog and digital beamforming appears to be an attractive solution that performs near optimum as fully digital beamforming with the reduced number of radio frequency chains. For example, [171] uses a gain focusing lens and a part of feeding antennas attached to the lens for pencil analog-beamforming to yield the best receive SNR, and after that, digital beamspace precoding and combining is performed. [172] proposes hierarchical multi-resolution beamforming codebooks to realize different antenna beamwidths with joint analog-digital processing, and [16] demonstrates the hybrid beamforming by hardware prototyping in microcellular mobile access. Recalling the fact that the eigen- and pencil-beamforming defined in Sect. 4.1 correspond to the fully digital and analog beamforming, the capacity difference between these two beamforming methods in Fig. 6(b) illustrates the benefit of introducing multiple radio frequency chains for capacity improvement. According to the result, installing multiple radio frequency chains improves the capacity if the Tx-Rx distance is below 3 m, while there is no point in doing that for beyond 3 m. When the digital beamforming is useful, the number of required radio frequency chains is determined by the SDoF. The entire antenna aperture is then divided into D_s segments, each of which is connected to the radio frequency chain and performs analog beamforming. It is worthwhile to mention that these design criteria are derived under an assumption that the antenna aperture including phase shifting mechanisms is lossless. Design of analog beamforming is also an important issue, since gain focusing does not necessarily lead to improved link capacity in time-varying channel conditions. Pencil beams may lose track and the communication overhead for the beam tracking may exceed the payload [180]. The use of less-directive antennas is suggested in [47] to increase the link availability in time-varying channels due to human movement in indoor office. For outdoor cellular scenarios, [71] indicates that an antenna with wide beamwidth at a ground level may lead to robust link budget in their rooftop-to-ground channel at 28 GHz, given the rich scattering and lack of beam tracking at the rooftop. Flattening antenna beams is proposed in [163] to cope with small variations of directional antenna orientation incurred by wind for mast-mounted outdoor backhaul links. Design of the hybrid beamforming under the presence of various losses and channel time-variation is of a practical interest for mm-wave devices.

5. Challenges Ahead in Mm-Wave Channel Modeling

Having reviewed the available mm-wave channel modeling and beamforming techniques, this section identifies essential but missing features of the channel model for the design and evaluation of mm-wave radios in the context of the 5G networks as defined in Sect. 1.

5.1 Multi-User and Multi-Site Channel Model

The mm-wave radios are most likely deployed as small

cells with dense installation over space. Even though the mm-wave radios have potential of spatial domain coexistence through beamforming, co-channel interference between neighboring cells will be a possible bottleneck as in the current cellular networks operated in the microwave frequency bands. Installing multiple mm-wave radio-heads or access points is also useful to attain the macro diversity [181]. Under the presence of human shadowing, probability of LOS visibility in indoor scenarios is analyzed in [182] for a varying number of access points, while [48] demonstrates low shadowing correlation between links for two access points widely separated in an aircraft cabin. Serving multiple users in a cellular context is covered in [95], where effects of correlation between different user-links on the sum-rate spectral efficiency is analyzed in detail. The inter-link correlation is attributed to physical scatterers that are commonly visible to multiple links such as highly elevated towers [103].

Spatial and shadowing correlation between different links in multi-user and multi-site settings is an essential feature in mm-wave radio networks relying on spatial coexistence through beamforming. Channel models covering the multi-link correlation at the mm-wave band have gained little attention so far, and the works analyzing the implication of the correlation on link performance are based on channel measurements and site-specific ray-tracing field prediction. Since the inter-link correlation at the mm-wave band seems to be more apparent than at the microwave band due to the directional selectivity of the channel [95], detailed studies on the link correlation would be required for mm-wave channel models. Geometry-based models introduced in Sect. 3.1.2 are vital bases for including the inter-link correlation since they can consider the physical scatterers that are common to multiple links and can control the inter-link correlation, as demonstrated at lower frequency bands [183]. However, parameterization of the model is presently lacking because of very few channel data that allow for it and rather involved parameterization procedure.

5.2 Dual Mobility Channel Model

The mm-wave radios are thought to play an essential role in high-rate wireless data transfer both in medium- and short-range scenarios. Focusing on the short-range applications, the mm-wave radio has originally been considered as an attractive physical layer scheme for device-to-device communications in the context of personal and local area networks [9], [10] such as for desktop environments. In these environments, motion of a device affects the channel and beamforming performance significantly [180] and a dual-mobility channel imposes the most significant deterioration to the link performance. The devices are furthermore in proximity to fixtures and human body, making the shadowing much more complex than the case of “devices in free space”; a proximity effect of mm-wave devices to human body on antenna radiation characteristics is demonstrated in [184]. Presently ray-based channel models are popularly ex-

ploited to produce the device-to-device channels with dual mobility such as for various indoor scenarios [86] and also in the military context [185]. Fully stochastic channel models such as the GSCMs usually have limited support of the dual mobility since they have been developed for ordinal mobile scenarios, where the base station is not supposed to move over time. Therefore environment-specific GSCMs have been proposed for dual-mobility channels, such as [186] defining a reference highway environment by placing scatterers in plausible locations to reproduce vehicle-to-vehicle channels. A recent work [187] proposes a dual-mobility GSCM for an urban environment, where the scatterer distribution follows a simplified geometry such as a street grid. These environment-specific reference GSCMs are used to reproduce channels at microwave frequencies, and are in principle applicable also to the mm-wave bands. However, building a layout of the reference environments and their parametrization, such as density of scatterers and their scattering properties, is not necessarily straightforward at the mm-wave band because of lack of supporting channel measurements.

5.3 Frequency-Unified Channel Model

The mm-wave radios are capable of providing the high-rate wireless data transfer provided that operating environments are favorable, such as low device mobility, low variation of the surrounding environment, and marginal link blockage. Feasibility of the mm-wave radios for highly time-variant and long-range scenarios is still an open question. For this purpose, radio links operating at the lower frequency bands are essential for possible fall-back options of the mm-wave radio links [5]. Presently no channel model is available to cover wide frequency ranges from microwave to mm-wave to reproduce *consistent* spatio-temporal channels. There are only a few papers that consider the correlation of channels at microwave and mm-wave frequencies. A seminal work [188] mentions that a basic propagation mechanism of the measured 40 and 60 GHz outdoor channels is similar, while the fading statistics are different from microwave mobile links due to fewer multipaths. Reported comparisons of channel characteristics at the mm-wave bands cover pathloss and delay spread with those measured at 2 GHz in office rooms [189], [190], 5 GHz in halls and meeting rooms [191], [192], 6.5 GHz in a car compartment [62], 17 GHz in an office building [193], [194] and in a car compartment [195], and finally with ultrawideband indoor channels [196], [197]. Comparison of channel characteristics parameters for different mm-wave frequency bands is reported in [27] for outdoor 38 and 60 GHz channels, [90] for indoor 60 and 70 GHz channels, and [21], [28] for 28 and 73 GHz in urban cellular channels. The papers tend to reveal that the equivalent omni-directional pathloss has similar pathloss exponents for mm-wave and microwave frequencies, and the main difference stems from the existence or absence of LOS that affects the initial pathloss. However, it is necessary to have much more measurements to justify this insight. Re-

cent extensive pathloss modeling at 2.2, 4.7, and 26.4 GHz in an urban microcellular scenario [110] demonstrates applicability of the pathloss model of the ITU report to 26.4 GHz channels to great extent, which are originally stated to be valid up to 6 GHz only [102].

The consistent multi-frequency spatio-temporal model requires multipath cluster properties to be a function of the radio carrier frequencies. The clusters are an essential part of both power spectrum models and GSCMs discussed in Sect. 3.1.2. The clustering can be performed either by relating the clusters with physical objects in propagation environments [68], [198], or on a multipath parameter space [88], [199] where the carrier frequency is added as a new dimension of the space. Here, again, there are very few multi-frequency channel measurements available to date to support the modeling activity.

6. Concluding Remarks

This paper first lists the roles of the mm-wave radio that make it an essential technological component for the realization of 5G mobile access and backhaul. The capabilities include multi-user and multi-site access, simultaneous handling of short-range mobile access and medium-range back or front-haul, support of moderate user mobility, and coordination with microwave frequency links. Properties of mm-wave radio and propagation channels influential to the identified capabilities are then summarized through a comprehensive literature survey. It is possible to deduce several *rules-of-thumb* concerning the properties of mm-wave radio channels; 1) typical pathloss exponents of equivalent omnidirectional channels are 1.7 and 3.3 in indoor LOS and NLOS scenarios, while those of outdoor cellular channels are 2.1 and between 2.7 and 4.6 in LOS and NLOS scenarios, respectively. Those exponents do not seem to differ across mm-wave frequency range, but do differ depending on the measurement environment; 2) delay spread is mostly less than 20 ns even in NLOS outdoor scenarios provided the antenna beams are directed towards the strongest multipath component. The delay spreads can be much higher when antenna beam misalignment occurs, which raises direct implication on link error performance; 3) typical normalized angular spread is around 0.55 and 0.8 in indoor LOS and NLOS channels, while very few results are available in outdoor environments; 4) coherence time of indoor radio channels under the human activity is up to 50 ms typically, while the human blockage can last up to a few hundred milliseconds in crowded indoor scenarios. The paper then addressed channel modeling frameworks with respect to stochastic and site-specific approaches. The former includes power spectrum models and geometry-based models, while the latter follows the ray-tracing and more recently the full-scattering method of wave propagation as exemplified in the indoor channel modeling. These channel modeling frameworks have their own strength and drawbacks, and therefore, it is meaningful to combine several of these frameworks to accomplish demanding channel modeling ac-

tivities. The joint use of measurements and site-specific field prediction allows us to interpolate and even extrapolate the measurements by the field prediction. Incorporating a characteristic geometry of the environment into a stochastic channel model yields reduction in computational complexity and improved accuracy of the reproduced channel as exemplified in the street-canyon scenario. The paper furthermore reviewed beamforming techniques as an essential enabler of the mm-wave radios. Design criteria of the hybrid analog-digital beamforming are developed based on the SDof and a comparison of the channel capacity with pencil- and eigen-beamforming, which are made possible through the expression of spatial *propagation* channels. Finally, essential but presently missing features of mm-wave channel models are identified; that is, 1) multi-user and multi-site model, 2) dual-mobility support, and 3) frequency-unified description. During possible actions to complement the features are discussed, it became apparent that mm-wave channel measurements and reliable channel prediction tools are very scarce to support the modeling activities. It is therefore crucial to promote collective actions on the mm-wave channel studies towards successful deployment of the mm-wave radio as a key technological element of the 5G mobile access and backhaul.

References

- [1] The METIS 2020 Project, "Laying the foundation of 5G." www.metis2020.com/
- [2] E. Violette, R. Espeland, R. DeBolt, and F. Schwering, "Millimeter-wave propagation at street level in an urban environment," *IEEE Trans. Geosci. Remote Sens.*, vol.26, no.3, pp.368–380, May 1988.
- [3] F.K. Schwering, E.J. Violette, and R.H. Espeland, "Millimeter-wave propagation in vegetation: Experiments and theory," *IEEE Trans. Geosci. Remote Sens.*, vol.26, no.3, pp.355–367, May 1988.
- [4] F. Giannetti, M. Luise, and R. Reggiannini, "Mobile and personal communications in the 60 GHz band: A survey," *Wirel. Pers. Commun.*, vol.10, no.2, pp.207–243, 1999.
- [5] P. Smulders, "Exploiting the 60 GHz band for local wireless multimedia access: Prospects and future directions," *IEEE Commun. Mag.*, vol.40, no.1, pp.140–147, Jan. 2002.
- [6] R.C. Daniels and R.W. Heath, "60 GHz wireless communications: Emerging requirements and design recommendations," *IEEE Veh. Technol. Mag.*, vol.2, no.3, pp.41–50, Sept. 2007.
- [7] FCC, "Allocations and service rules for the 71–76 GHz, 81–86 GHz, and 92–95 GHz bands," FCC Memorandum Opinion and Order 05–45, Federal Communications Commission, Washington D.C., 2005.
- [8] ECC, "Radio frequency channel arrangements for fixed service systems operating in the bands 71–76 GHz and 81–86 GHz," ECC Recommendation (05)07, Electronic Communications Committee, 2005.
- [9] IEEE, "Wireless medium access control (MAC) and physical layer (PHY) specifications for high rate wireless personal area networks (WPANs) amendment 2: Millimeter-wave-based alternative physical layer extension." *IEEE Standard 802.15.3c-2009*, 2009.
- [10] IEEE, "Part 11: Wireless LAN Medium Access Control (MAC) and Physical Layer (PHY) specifications amendment 3: Enhancements for very high throughput in the 60 GHz band," *IEEE Standard 802.11ad-2012*, 2012.
- [11] WirelessHD, "The first 60 GHz standard," www.wirelesshd.org/

- [12] Wi-Fi alliance, "The worldwide network of companies that brings you Wi-Fi," www.wi-fi.org/
- [13] D. Lockie and D. Peck, "High-data-rate millimeter-wave radios," *IEEE Micro Mag.*, vol.10, no.5, pp.75–83, Aug. 2009.
- [14] T.S. Rappaport et al., "Millimeter wave mobile communications for 5G cellular: It will work!," *IEEE Access*, vol.1, pp.335–349, 2013.
- [15] S. Rangan, T.S. Rappaport, and E. Erkip, "Millimeter-wave cellular wireless networks: Potentials and challenges," *Proc. IEEE*, vol.102, no.3, pp.366–385, March 2014.
- [16] W. Roh et al., "Millimeter-wave beamforming as an enabling technology for 5G cellular communications: theoretical feasibility and prototype results," *IEEE Commun. Mag.*, vol.52, pp.106–113, Feb. 2014.
- [17] J. Medbo et al., "Channel modeling for the fifth generation mobile communications," *Proc. 8th European Conf. Antennas Propag. (EuCAP2014)*, Den Haag, the Netherlands, pp.1–5, April 2014.
- [18] M. Steinbauer, A.F. Molisch, and E. Bonek, "The double-directional radio channel," *IEEE Antennas Propag. Mag.*, vol.43, no.4, pp.51–63, Aug. 2001.
- [19] P. Bello, "Characterization of randomly time-variant linear channels," *IEEE Trans. Commun. Syst.*, vol.11, no.4, pp.360–393, Dec. 1963.
- [20] A. Molisch, *Wireless Communications*, 2nd ed., Wiley, 2010.
- [21] G.R. MacCartney, M.K. Samimi, and T.S. Rappaport, "Omnidirectional path loss models in New York City at 28 GHz and 73 GHz," *Proc. 20th IEEE Int. Symp. Personal, Indoor and Mobile Radio Commun. (PIMRC 2009)*, Washington DC, Sept. 2014.
- [22] P.F.M. Smulders, "Statistical characterization of 60-GHz indoor radio channels," *IEEE Trans. Antennas Propag.*, vol.57, no.10, pp.2820–2829, Oct. 2009.
- [23] H. Thomas, R. Cole, and G. Siqueira, "An experimental study of the propagation of 55 GHz millimeter waves in an urban mobile radio environment," *IEEE Trans. Veh. Technol.*, vol.43, no.1, pp.140–146, Feb. 1994.
- [24] M. Samimi et al., "28 GHz angle of arrival and angle of departure analysis for outdoor cellular communications using steerable beam antennas in New York city," *Proc. 77th IEEE Veh. Technol. Conf. (VTC 2013-Spring)*, pp.1–6, June 2013.
- [25] Y. Azar et al., "28 GHz propagation measurements for outdoor cellular communications using steerable beam antennas in New York city," *Proc. 2013 IEEE Int. Conf. Commun. (ICC 2013)*, pp.5143–5147, June 2013.
- [26] E. Ben-Dor et al., "Millimeter-wave 60 GHz outdoor and vehicle AOA propagation measurements using a broadband channel sounder," *Proc. IEEE Global Telecommun. Conf. (GLOBECOM 2011)*, pp.1–6, Dec. 2011.
- [27] T.S. Rappaport, E. Ben-Dor, J.N. Murdock, and Q. Yijun, "38 GHz and 60 GHz angle-dependent propagation for cellular & peer-to-peer wireless communications," *Proc. IEEE Int. Conf. Commun. (ICC 2012)*, pp.4568–4573, June 2012.
- [28] M.R. Akdeniz et al., "Millimeter wave channel modeling and cellular capacity evaluation," *IEEE J. Sel. Areas Commun.*, vol.6, no.6, pp.1164–1179, Sept. 2014.
- [29] G.R. MacCartney, J. Zhang, S. Nie, and T.S. Rappaport, "Path loss models for 5G millimeter wave propagation channels in urban microcells," *Proc. 2013 IEEE Global Commun. Conf. (GLOBECOM 2013)*, pp.3948–3953, Dec. 2013.
- [30] A.I. Sulyman et al., "Radio propagation path loss models for 5G cellular networks in the 28 GHz and 38 GHz millimeter-wave bands," *IEEE Commun. Mag.*, vol.52, no.9, pp.78–86, Sept. 2014.
- [31] T. Bai, V. Desai, and R. Heath, "Millimeter wave cellular channel models for system evaluation," *Proc. Int. Conf. Computing, Netw. Commun. (ICNC 2014)*, pp.178–182, Feb. 2014.
- [32] P. Watson, "Modelling radio propagation at millimetre-wave-lengths for communications and remote sensing," *Proc. IEE 7th Int. Conf. Antennas Propag. (ICAP 1991)*, pp.269–273, April 1991.
- [33] P. Papazian, G.A. Hufford, R. Achatz, and R. Hoffman, "Study of the local multipoint distribution service radio channel," *IEEE Trans. Broadcast.*, vol.43, no.2, pp.175–184, June 1997.
- [34] P.F.M. Smulders and L.M. Correia, "Characterisation of propagation in 60 GHz radio channels," *IEE Electron. Commun. Eng. J.*, vol.9, no.2, pp.73–80, April 1997.
- [35] M. Al-Nuaimi and R.B.L. Stephens, "Measurements and prediction model optimisation for signal attenuation in vegetation media at centimetre wave frequencies," *IEE Microw. Antennas Propag.*, vol.145, no.3, pp.201–206, June 1998.
- [36] H. Xu, T. Rappaport, R. Boyle, and J. Schaffner, "Measurements and models for 38-GHz point-to-multipoint radiowave propagation," *IEEE J. Sel. Areas Commun.*, vol.18, no.3, pp.310–321, March 2000.
- [37] S.A. Khan, A.N. Tawfik, C.J. Gibbins, and B.C. Gremont, "Extra-high frequency line-of-sight propagation for future urban communications," *IEEE Trans. Antennas Propag.*, vol.51, no.11, pp.3109–3121, Nov. 2003.
- [38] Q. Zhao and L. Jin, "Rain attenuation in millimeter wave ranges," *Proc. 7th Int. Symp. Antennas Propag. EM Theory (ISAPE '06)*, pp.1–4, Oct. 2006.
- [39] T. Tjelta and T.O. Breivik, "Measured attenuation data and predictions for a gigabit radio link in the 80 GHz band," *Proc. 3rd European Conf. Antennas Propag. (EuCAP 2009)*, pp.657–661, March 2009.
- [40] J. Hansryd, L. Yinggang, C. Jingjing, and P. Ligander, "Long term path attenuation measurement of the 71–76 GHz band in a 70/80 GHz microwave link," *Proc. 4th European Conf. Antennas Propag. (EuCAP 2010)*, pp.1–4, April 2010.
- [41] International Telecommunication Union, "Specific attenuation model for rain for use in prediction methods," *Recommendation ITU-R P.838-3*, 2005.
- [42] International Telecommunication Union, "Attenuation due to clouds and fog," *Recommendation ITU-R P.840-6*, Sept. 2013.
- [43] S. Geng, J. Kivinen, X. Zhao, and P. Vainikainen, "Millimeter-wave propagation channel characterization for short-range wireless communications," *IEEE Trans. Veh. Technol.*, vol.58, no.1, pp.3–13, Jan. 2009.
- [44] H. Zhao et al., "28 GHz millimeter wave cellular communication measurements for reflection and penetration loss in and around buildings in New York city," *Proc. IEEE Int. Conf. Commun. (ICC)*, pp.5163–5167, June 2013.
- [45] S. Takahashi, A. Kato, K. Sato, and M. Fujise, "Distance dependence of path loss for millimeter wave inter-vehicle communications," *Proc. IEEE 58th Veh. Technol. Conf. (VTC 2003-Fall)*, pp.26–30, Oct. 2003.
- [46] A. Yamamoto et al., "Path-loss prediction models for intervehicle communication at 60 GHz," *IEEE Trans. Veh. Technol.*, vol.57, no.1, pp.65–78, Jan. 2008.
- [47] S. Collonge, G. Zaharia, and G. Zein, "Influence of the human activity on wide-band characteristics of the 60 GHz indoor radio channel," *IEEE Trans. Wireless Commun.*, vol.3, no.6, pp.2396–2406, Nov. 2004.
- [48] A. Garcia et al., "60 GHz time-variant shadowing characterization within an airbus 340," *Proc. 4th European Conf. Antennas Propag. (EuCAP 2010)*, pp.1–5, April 2010.
- [49] N. Moraitis and P. Constantinou, "Indoor channel measurements and characterization at 60 GHz for wireless local area network applications," *IEEE Trans. Antennas Propag.*, vol.52, no.12, pp.3180–3189, Dec. 2004.
- [50] P. Marinier, G.Y. Delisle, and C. Despins, "Influence of human motion on indoor wireless millimeter-wave channel characteristics," *Proc. IEEE 47th Veh. Technol. Conf. (VTC 1997)*, pp.979–983, May 1997.
- [51] P. Marinier, G.Y. Delisle, and C. Despins, "Temporal variations of the indoor wireless millimeter-wave channel," *IEEE Trans. Anten-*

- nas Propag., vol.46, no.6, pp.928–934, June 1998.
- [52] T. Manabe et al., “Multipath measurement at 60 GHz for indoor wireless communication systems,” Proc. IEEE 44th Veh. Technol. Conf. (VTC 1994), pp.905–909, June 1994.
- [53] T. Manabe, Y. Miura, and T. Ihara, “Effects of antenna directivity and polarization on indoor multipath propagation characteristics at 60 GHz,” IEEE J. Sel. Areas Commun., vol.14, no.3, pp.441–448, April 1996.
- [54] T. Manabe et al., “Polarization dependence of multipath propagation and high-speed transmission characteristics of indoor millimeter-wave channel at 60 GHz,” IEEE Trans. Veh. Technol., vol.44, no.2, pp.268–274, May 1995.
- [55] C. Loyez, N. Rolland, P.A. Rolland, and O. Lafond, “Indoor 60 GHz radio channel sounding and related T/R module considerations for high data rate communications,” Electron. Lett., vol.37, no.10, pp.654–655, May 2001.
- [56] U. Karthaus and R. Noe, “Influence of polarization on 30 GHz broadband radio channels,” Proc. 1998 Int. Zurich Sem. Broadband Communications, pp.159–164, Feb. 1998.
- [57] N. Daniele, D. Chagnot, and C. Fort, “Outdoor millimetre-wave propagation measurements with line of sight obstructed by natural elements,” Electron. Lett., vol.30, no.18, pp.1533–1534, Sept. 1994.
- [58] G. Lovnes, J. Reis, and R. Raekken, “Channel sounding measurements at 59 GHz in city streets,” Proc. 5th IEEE Int. Symp. Personal, Indoor and Mobile Radio Commun. (PIMRC 94), pp.496–500, Sept. 1994.
- [59] T.S. Rappaport et al., “Broadband millimeter-wave propagation measurements and models using adaptive-beam antennas for outdoor urban cellular communications,” IEEE Trans. Antennas Propag., vol.61, no.4, pp.1850–1859, April 2013.
- [60] S. Sun and T.S. Rappaport, “Wideband mmwave channels: Implications for design and implementation of adaptive beam antennas,” Proc. 2014 IEEE Int. Microwave Symp. (IMS2014), pp.1–4, June 2014.
- [61] M. Kyro, Radio wave propagation and antennas for millimeter-wave communications, Ph.D. thesis, Aalto University, Espoo, Finland, Nov. 2012.
- [62] R. Nakamura and A. Kajiwara, “Empirical study on 60 GHz in-vehicle radio channel,” Proc. IEEE Radio and Wireless Symp. (RWS 2012), pp.327–330, Jan. 2012.
- [63] M. Peter, R. Felbecker, W. Keusgen, and J. Hillebrand, “Measurement-based investigation of 60 GHz broadband transmission for wireless in-car communication,” Proc. 70th IEEE Veh. Technol. Conf. (VTC 2009-Fall), pp.1–5, Sept. 2009.
- [64] M. Peter, W. Keusgen, A. Kortke, and M. Schirrmacher, “Measurement and analysis of the 60 GHz in-vehicular broadband radio channel,” Proc. IEEE 66th Veh. Technol. Conf. (VTC 2007-Fall), pp.834–838, Sept. 2007.
- [65] T. Zwick, T.J. Beukema, and H. Nam, “Wideband channel sounder with measurements and model for the 60 GHz indoor radio channel,” IEEE Trans. Veh. Technol., vol.54, no.4, pp.1266–1277, July 2005.
- [66] H. Xu, V. Kukshya, and T. Rappaport, “Spatial and temporal characteristics of 60-GHz indoor channels,” IEEE J. Sel. Areas Commun., vol.20, no.3, pp.620–630, April 2002.
- [67] N. Moraitis, P. Constantinou, and D. Vouyioukas, “Power angle profile measurements and capacity evaluation of a SIMO system at 60 GHz,” Proc. IEEE 21st Int. Symp. Personal Indoor and Mobile Radio Commun. (PIMRC 2010), pp.1027–1031, Sept. 2010.
- [68] C. Gustafson, F. Tufvesson, S. Wyne, K. Haneda, and A.F. Molisch, “Directional analysis of measured 60 GHz indoor radio channels using SAGE,” Proc. IEEE 73rd Veh. Technol. Conf. (VTC 2011-Spring), pp.1–6, Budapest, Hungary, May 2011.
- [69] M.T. Martinez-Ingles et al., “Deterministic and experimental indoor mmw channel modeling,” IEEE Ant. Wireless Prop. Lett., vol.13, pp.1047–1050, 2014.
- [70] D. Dupleich et al., “Directional characterization of the 60 GHz indoor-office channel,” Proc. 2014 XXXIth URSI General Assembly and Scientific Symp. (URSI GASS 2014), pp.1–4, Aug. 2014.
- [71] S. Rajagopal, S. Abu-Surra, and M. MalmirChegini, “Channel feasibility for outdoor non-line-of-sight mmwave mobile communication,” Proc. IEEE Veh. Technol. Conf. (VTC 2012 Fall), pp.1–6, Sept. 2012.
- [72] A.A.M. Saleh and R.A. Valenzuela, “A statistical model for indoor multipath propagation,” IEEE J. Sel. Areas Commun., vol.5, no.2, pp.128–137, Feb. 1987.
- [73] Q. Spencer, B. Jeffs, M. Jensen, and A. Swindlehurst, “Modeling the statistical time and angle of arrival characteristics of an indoor multipath channel,” IEEE J. Sel. Areas Commun., vol.18, no.3, pp.347–360, March 2000.
- [74] P.F.M. Smulders, Broadband wireless LANs: A feasibility study, Ph.D. thesis, Eindhoven Univ. of Tech., The Netherlands, 1995.
- [75] J. Park, Y. Kim, Y. Hur, K. Lim, and K. Kim, “Analysis of 60 GHz band indoor wireless channels with channel configurations,” Proc. 9th IEEE Int. Symp. Personal, Indoor and Mobile Radio Commun. (PIMRC 98), pp.617–620, Sept. 1998.
- [76] J. Kunisch, E. Zollinger, J. Pamp, and A. Winkelmann, “Median 60 GHz wideband indoor radio channel measurements and model,” Proc. IEEE 50th Veh. Technol. Conf. (VTC 1999 Fall), pp.2393–2397, Amsterdam, the Netherlands, Sept. 1999.
- [77] J. Hubner, S. Zeisberg, K. Koora, J. Borowski, and A. Finger, “Simple channel model for 60 GHz indoor wireless LAN design based on complex wideband measurements,” Proc. IEEE 47th Veh. Technol. Conf., pp.1004–1008, May 1997.
- [78] P. Soma, C. Ong, S. Sun, and M.Y.W. Chia, “Propagation measurements and modeling of LMDS radio channel in singapore,” IEEE Trans. Veh. Technol., vol.52, no.3, pp.595–606, May 2003.
- [79] Y. Shoji, H. Sawada, C.S. Choi, and H. Ogawa, “A modified SV-model suitable for line-of-sight desktop usage of millimeter-wave WPAN systems,” IEEE Trans. Antennas Propag., vol.57, no.10, pp.2940–2948, Oct. 2009.
- [80] K. Sato, H. Sawada, Y. Shoji, and S. Kato, “Channel model for millimeter wave WPAN,” Proc. IEEE 18th Int. Symp. Personal, Indoor and Mobile Radio Commun. (PIMRC 2007), pp.1–5, Sept. 2007.
- [81] C. Liu, E. Skafidas, and R. Evans, “Angle of arrival extended S-V model for the 60 GHz wireless indoor channel,” Proc. Australasian Telecommun. Netw. Applicat. Conf. (ATNAC 2007), pp.181–185, Dec. 2007.
- [82] A. Maltsev et al., “Experimental investigations of 60 GHz WLAN systems in office environment,” IEEE J. Sel. Areas Commun., vol.27, no.8, pp.1488–1499, Oct. 2009.
- [83] A. Maltsev et al., “Statistical channel model for 60 GHz wlan systems in conference room environment,” Radioengineering, June 2011.
- [84] H. Sawada, H. Nakase, K. Sato, and H. Harada, “A sixty GHz vehicle area network for multimedia communications,” IEEE J. Sel. Areas Commun., vol.27, no.8, pp.1500–1506, Oct. 2009.
- [85] S.K. Yong, 60 GHz Channel Characterizations and Modeling, pp.17–61, John Wiley & Sons, 2010.
- [86] A. Maltsev et al., “Channel models for 60 GHz WLAN systems,” IEEE802.11-09/0334r3, July 2009.
- [87] D. Cassioli, “60 GHz UWB channel measurement and model,” Proc. 2012 IEEE Int. Conf. Ultra-Wideband (ICUWB 2012), pp.145–149, Syracuse, NY, Sept. 2012.
- [88] C. Gustafson, K. Haneda, S. Wyne, and F. Tufvesson, “On mm-wave multipath clustering and channel modeling,” IEEE Trans. Antennas Propag., vol.62, no.3, pp.1445–1455, March 2014.
- [89] M. Kyro et al., “Statistical channel models for 60 GHz radio propagation in hospital environments,” IEEE Trans. Antennas Propag., vol.60, no.3, pp.1569–1577, March 2012.
- [90] K. Haneda, J. Jarvelainen, A. Karttunen, A. Kyro, and J. Putkonen, “A statistical spatio-temporal radio channel model for large indoor

- environments at 60 and 70 GHz,” *IEEE Trans. Antennas Propag.*, vol.63, no.6, June 2015, in press.
- [91] A. Richter, Estimation of radio channel parameters: Models and algorithms, Ph.D. Thesis, Technische Universitat Ilmenau, Germany, 2005.
- [92] K. Haneda, J. Jarvelainen, A. Karttunen, M. Kyro, and J. Putkonen, “Indoor short-range radio propagation measurements at 60 and 70 GHz,” *Proc. 8th European Conf. Antennas Propag. (EuCAP2014)*, pp.1–5, Den Haag, the Netherlands, April 2014.
- [93] M.S. Choi, G. Grosskopf, and D. Rohde, “Statistical characteristics of 60 GHz wideband indoor propagation channel,” *Proc. 2005 IEEE 16th Personal, Indoor and Mobile Radio Commun. (PIMRC 2005)*, pp.599–603, Sept. 2005.
- [94] S. Sun and T.S. Rappaport, “Multibeam antenna combining for 28 GHz cellular link improvement in urban environments,” *Proc. IEEE Global Telecommun. Conf. (GLOBECOM 2014)*, pp.5468–5473, Austin, TX, Dec. 2014.
- [95] A. Adhikary et al., “Joint spatial division and multiplexing for mm-wave channels,” *IEEE J. Sel. Areas Commun.*, vol.32, no.6, pp.1239–1255, June 2014.
- [96] V. Erceg et al., “TGN channel models,” *IEEE 802.11-03/940r4*, May 2004.
- [97] A. Karttunen, K. Haneda, J. Jarvelainen, and J. Putkonen, “Polarisation characteristics of propagation paths in indoor 70 GHz channels,” *Proc. 9th European Conf. Antennas Propag. (EuCAP 2015)*, MA11-6, Lisbon, Portugal, April 2015.
- [98] C. Gustafson, 60 GHz wireless propagation channels: Characterization, modeling and evaluation, Ph.D. thesis, Lund University, Sweden, 2014.
- [99] L. Liu et al., “The cost 2100 MIMO channel model,” *IEEE Wireless Commun.*, vol.19, no.6, pp.92–99, Dec. 2012.
- [100] P. Kyosti et al., “WINNER II channel models, D1.1.2,” <https://www.ist-winner.org/WINNER2-Deliverables/D1.1.2v1.1.pdf>, 2007.
- [101] 3GPP TR 25.996, “Spatial channel model for multiple input multiple output (MIMO) simulations,” Dec. 2009.
- [102] International Telecommunication Union, “Guidelines for evaluation of radio interface technologies for IMT-Advanced,” Report ITU-R M.2135-1, Dec. 2009.
- [103] K. Kalliola et al., “3-D double-directional radio channel characterization for urban macrocellular applications,” *IEEE Trans. Antennas Propag.*, vol.51, no.11, pp.3122–3133, Nov. 2003.
- [104] J. Zhang, J. Richter, L. Ivrisimtzis, and M. Al-Nuaimi, “Statistical modelling at 20 GHz for fixed wireless access systems in urban multipath environments,” *IEE Proc. Micro., Antennas Propag.*, vol.152, no.4, pp.278–283, Aug. 2005.
- [105] L. Ivrisimtzis, M. Al-Nuaimi, J. Richter, and J. Zhang, “A statistical model of the urban propagation channel in fixed wireless systems,” *Proc. Int. Union of Radio Science 27th General Assembly (URSI 2002)*, CAFO.7, Maastricht, Netherlands, Aug. 2002.
- [106] J. Zhang, J. Richter, L. Ivrisimtzis, and M. Al-Nuaimi, “Measurements and modelling for fixed wireless access systems at millimeter wave frequencies,” *Proc. 12th Int. Conf. Antennas Propag. (ICAP 2003)*, pp.433–436, March 2003.
- [107] M. Kyro et al., “Long range wideband channel measurements at 81–86 GHz frequency range,” *Proc. 4th European Con. Ant. Propagation (EuCAP 2010)*, pp.1–5, April 2010.
- [108] M. Kyro, V. Kolmonen, and P. Vainikainen, “Experimental propagation channel characterization of mm-wave radio links in urban scenarios,” *IEEE Ant. Wireless Prop. Lett.*, vol.11, pp.865–868, 2012.
- [109] M.K. Samimi and T.S. Rappaport, “Ultra-wideband statistical channel model for non line of sight millimeter-wave urban channels,” *Proc. IEEE Global Telecommun. Conf. (GLOBECOM 2014)*, pp.3483–3489, Austin, TX, Dec. 2014.
- [110] T. Jamsa et al., “Deliverable D1.2 initial channel models based on measurements,” https://www.metis2020.com/wp-content/uploads/deliverables/METIS_D1.2_v1.pdf, 2014.
- [111] M.T. Martinez-Ingles et al., “Comparison of a UTD-PO formulation for multiple-plateau diffraction with measurements at 62 GHz,” *IEEE Trans. Antennas Propag.*, vol.61, no.2, pp.1000–1003, Feb. 2013.
- [112] M.T. Martinez-Ingles et al., “Parametric study and validation of a UTD-PO multiple-cylinder diffraction solution through measurements at 60 GHz,” *IEEE Trans. Antennas Propag.*, vol.61, no.8, pp.4397–4400, Aug. 2013.
- [113] M. Martinez-Ingles et al., “UTD-PO solution for estimating the propagation loss due to the diffraction at the top of a rectangular obstacle when illuminated from a low source,” *IEEE Trans. Antennas Propag.*, vol.61, no.12, pp.6247–6250, Dec. 2013.
- [114] M. Jacob et al., “Diffraction in mm and sub-mm wave indoor propagation channels,” *IEEE Trans. Microw. Theory Tech.*, vol.60, no.3, pp.833–844, March 2012.
- [115] A. Maltsev et al., “Characteristics of indoor millimeter-wave channel at 60 GHz in application to perspective WLAN system,” *Proc. 4th European Conf. Antennas Propag. (EuCAP 2010)*, pp.1–5, April 2010.
- [116] T. Manabe, K. Sato, and T. Ihara, “Measurement of complex refractive index of soda-lime glass at 60 GHz by vector-network-analyser-based scatterometer,” *Electron. Lett.*, vol.28, no.14, pp.1354–1355, July 1992.
- [117] B. Langen, G. Lober, and W. Herzig, “Reflection and transmission behaviour of building materials at 60 GHz,” *Proc. IEEE Int. Symp. Personal, Indoor and Mobile Radio Commun. (PIMRC 1994)*, pp.505–509, Sept. 1994.
- [118] L. Correia and P. Frances, “Estimation of materials characteristics from power measurements at 60 GHz,” *Proc. IEEE Int. Symp. Personal, Indoor and Mobile Radio Commun. (PIMRC 1994)*, pp.510–513, Sept. 1994.
- [119] L. Correia and P. Frances, “Transmission and isolation of signals in buildings at 60 GHz,” *Proc. 6th IEEE Personal, Indoor and Mobile Radio Commun. (PIMRC’95)*, pp.1031–1034, Sept. 1995.
- [120] K. Sato et al., “Measurements of reflection characteristics and refractive indices of interior construction materials in millimeter-wave bands,” *Proc. 45th IEEE Veh. Technol. Conf. (VTC 1995)*, pp.449–453, July 1995.
- [121] J. Lahteenmaki and T. Karttaavi, “Measurement of dielectric parameters of wall materials at 60 GHz band,” *Electron. Lett.*, vol.32, no.16, pp.1442–1444, Aug. 1996.
- [122] K. Sato et al., “Measurement of the complex refractive index of concrete at 57.5 GHz,” *IEEE Trans. Antennas Propag.*, vol.44, no.1, pp.35–40, Jan. 1996.
- [123] L. Li, Y. Wang, and K. Gong, “Measurements of building construction materials at Ka band,” *Int. J. Infrared Millim. Waves*, vol.19, no.9, pp.1293–1298, Dec. 1998.
- [124] H. Radi, M. Fiocco, M.A.N. Parks, and S.R. Saunders, “Simultaneous indoor propagation measurements at 17 and 60 GHz for wireless local area networks,” *Proc. 48th IEEE Veh. Technol. Conf. (VTC 1998)*, pp.510–514, May 1998.
- [125] I. Cuinas, J. Pugliese, A. Hammoudeh, and M. Sanchez, “Frequency dependence of dielectric constant of construction materials in the microwave and millimeter wave bands,” *Microw. Opt. Tech. Lett.*, vol.30, no.2, pp.123–124, July 2000.
- [126] C. Anderson and T. Rappaport, “In-building wideband partition loss measurements at 2.5 and 60 GHz,” *IEEE Trans. Wirel. Commun.*, vol.3, no.3, pp.922–928, May 2004.
- [127] A. Alejos, M. Sanchez, and I. Cuinas, “Measurement and analysis of propagation mechanisms at 40 GHz: Viability of site shielding forced by obstacles,” *IEEE Trans. Veh. Technol.*, vol.57, no.6, pp.3369–3380, Nov. 2008.
- [128] J. Ahmadi-Shokouh, S. Noghianian, E. Hossain, M. Ostadrahimi, and J. Dietrich, “Reflection coefficient measurement for house flooring materials at 57–64 GHz,” *Proc. 2009 IEEE Global Telecommun. Conf. (GLOBECOM 2009)*, pp.1–6, Nov. 2009.

- [129] C. DeVries, J. Deforge, and D. Badiere, "Predicting indoor performance of a 60 GHz WPAN," Proc. 2013 IEEE Radio and Wireless Symp. (RWS 2013), pp.157–159, Jan. 2013.
- [130] M. Kyro, V. Semkin, and V. Kolmonen, "Empirical characterization of scattering pattern of built surfaces at mm-wave frequencies," Proc. 7th European Conf. Antennas Propag. (EuCAP 2013), pp.112–115, April 2013.
- [131] International Telecommunication Union, "Propagation data and prediction methods for the planning of indoor radiocommunication systems and radio local area networks in the frequency range 900 MHz to 100 GHz," Recommendation ITU-R P.1238-7, Feb. 2012.
- [132] F. Villanese, N. Evans, and W. Scanlon, "Pedestrian-induced fading for indoor channels at 2.45, 5.7 and 62 GHz," Proc. 52nd IEEE Veh. Technol. Conf. (VTC 2000-Fall), pp.43–48, 2000.
- [133] M. Jacob et al., "A ray tracing based stochastic human blockage model for the IEEE 802.11ad 60 GHz channel model," Proc. 5th European Conf. Antennas Propag. (EuCAP2011), pp.3084–3088, Rome, Italy, April 2011.
- [134] L.M. Correia and J.R. Reis, "Wideband characterisation of the propagation channel for outdoors at 60 GHz," Proc. 7th IEEE Int. Symp. Personal, Indoor and Mobile Radio Commun. (PIMRC'96), pp.752–755, Oct. 1996.
- [135] M. Lecours, D. Grenier, M. Baqarhi, and S. Cherkaoui, "Measurements and simulation of received signals in rooms and corridors at 900 MHz and in the 20–60 GHz band," Proc. IEEE 43rd Veh. Technol. Conf. (VTC 1993), pp.871–874, May 1993.
- [136] A.M. Hammoudeh and G. Allen, "Millimetric wavelengths radiowave propagation for line-of-sight indoor microcellular mobile communications," IEEE Trans. Veh. Technol., vol.44, no.3, pp.449–460, Aug. 1995.
- [137] C. Ghobadi, P.R. Shepherd, and S.R. Pennock, "An improved 2-D model for indoor radio propagation at mm frequencies," Proc. IEEE Colloquium, Radio Commun. at Micro. Millimetre Wave Freq., pp.11/1–11/6, Dec. 1996.
- [138] C. Ghobadi, P.R. Shepherd, and S.R. Pennock, "2D ray-tracing model for indoor radio propagation at millimetre frequencies, and the study of diversity techniques," IEEE Proc. Microwaves, Antennas Propag., vol.145, no.4, pp.349–353, Aug. 1998.
- [139] C. Oestges and D. Vanhoenacker-Janvier, "Experimental validation and system applications of ray-tracing model in built-up areas," Electron. Lett., vol.36, no.5, pp.461–462, March 2000.
- [140] G. Riva, V. Degli-Esposti, E. De Ponti, L. Ferrucci, and E. Papa, "Characterization of mm-wave indoor propagation with directive antennas," Proc. 27th European Microwave Conf. (EuMC 97), pp.130–134, Sept. 1997.
- [141] C.P. Lim, M. Lee, R. Burkholder, J. Volakis, and R. Marhefka, "60 GHz indoor propagation studies for wireless communications based on a ray-tracing method," EURASIP J. Wireless Commun. Netw., 2007.
- [142] Y. Lostanlen et al., "Comparison of measurements and simulations in indoor environments for wireless local networks at 60 GHz," Proc. IEEE 55th Veh. Technol. Conf. (VTC 2002 Spring), pp.389–393, 2002.
- [143] B. Neekzad, K. Sayrafian-Pour, J. Perez, and J.S. Baras, "Comparison of ray tracing simulations and millimeter wave channel sounding measurements," Proc. IEEE 18th Int. Symp. Personal, Indoor and Mobile Radio Commun. (PIMRC 2007), pp.1–5, Sept. 2007.
- [144] J.J.G. Fernandes, P.F.M. Smulders, and J.C. Neves, "Simulation results on mm-wave indoor radio channel modelling and comparison with measurements," Proc. IEEE Second Symp. Commun. Veh. Technol. in the Benelux, pp.89–94, Nov. 1994.
- [145] J. Jarvelainen and K. Haneda, "Sixty gigahertz indoor radio wave propagation prediction based on full scattering model," Radio Sci., vol.49, pp.293–305, April 2014.
- [146] S. Collogne, G. Zaharia, and G. El Zein, "Experimental investigation of the spatial and temporal characteristics of the 60 GHz radio propagation within residential environments," Proc. Int. Symp. Signals, Circuits and Sys. (SCS 2003), pp.417–420, 2003.
- [147] M. Dinis, J. Garcia, V. Monteiro, and N. Oliveira, "Millimetre-wave channel impulse response measurements and comparison with ray-tracing simulation results," Proc. 13th IEEE Int. Symp. Personal, Indoor and Mobile Radio Commun. (PIMRC 2002), pp.463–467, Sept. 2002.
- [148] R. Tahri et al., "Spatial characterization of 60 GHz indoor channels by fast gaussian beam tracking method and comparison with measurements," Proc. IEEE 63rd Veh. Technol. Conf. (VTC 2006-Spring), pp.2722–2726, May 2006.
- [149] W. Peter, W. Keusgen, and R. Felbecker, "Measurement and ray-tracing simulation of the 60 GHz indoor broadband channel: Model accuracy and parameterization," Proc. Second European Conf. Antennas Propag. (EuCAP 2007), pp.1–8, Nov. 2007.
- [150] M.T. Martinez-Ingles et al., "Initial experimental characterization of the millimeter-wave radio channel," Proc. 6th European Conf. Antennas Propag. (EuCAP 2012), pp.1118–1120, March 2012.
- [151] M.T. Martinez-Ingles et al., "Indoor radio channel characterization at 60 GHz," Proc. 7th European Conf. Antennas Propag. (EuCAP 2013), pp.2796–2799, April 2013.
- [152] Y. Kim, K. Yang, and S. Kim, "Scattering characteristics of surface roughness in frequency and incident angle dependent at millimeter-wave," Proc. 1999 Asia Pacific Microw. Conf. (APMC 1999), pp.789–792, 1999.
- [153] C. Dillard, T. Gallagher, C. Bostian, and D. Sweeney, "Rough surface scattering from exterior walls at 28 GHz," IEEE Trans. Antennas Propag., vol.52, no.12, pp.3173–3179, Dec. 2004.
- [154] M.W. Jung, J. Kim, Y. Yoon, J.W. Kim, and S. Kim, "Enhancement approach of ray-tracing algorithm for propagation prediction at the mm-wave band," Proc. 35th Int. Conf. Infrared Millimeter and Terahertz Waves (IRMMW-THz 2010), pp.1–2, Sept. 2010.
- [155] Z. Muhi-Eldeen, L. Ivrisimtzis, and M. Al-Nuaimi, "Modelling and measurements of millimetre wavelength propagation in urban environments," IET Microw. Antennas Propag., vol.4, no.9, pp.1300–1309, Sept. 2010.
- [156] D. Mavrikakis and S.R. Saunders, "A delay-centred wideband indoor channel model for mm-wave communications," Proc. 12th Int. Conf. Antennas Propag. (ICAP 2003), pp.518–521, March 2003.
- [157] J. Jarvelainen et al., "60 GHz radio wave propagation prediction in a hospital environment using an accurate room structural model," Proc. 2014 Loughborough Conf. Antennas Propag. (LAPC 2012), pp.1–4, Nov. 2012.
- [158] J. Jarvelainen, M. Kurkela, A. Karttunen, K. Haneda, and J. Putkonen, "70 GHz radio wave propagation prediction in a large office," Proc. 2012 Loughborough Conf. Antennas Propag. (LAPC 2014), pp.420–424, Loughborough, UK, Nov. 2014.
- [159] V. Degli-Esposti, F. Fuschini, E.M. Vitucci, and G. Falciasecca, "Measurement and modelling of scattering from buildings," IEEE Trans. Antennas Propag., vol.55, no.1, pp.143–153, Jan. 2007.
- [160] X. An et al., "Beam switching support to resolve link-blockage problem in 60 GHz WPANs," Proc. IEEE Int. Symp. Personal, Indoor Mobile Radio Commun. (PIMRC 2009), pp.390–394, Tokyo, Japan, Sept. 2009.
- [161] J. Wang et al., "Beam codebook based beamforming protocol for multi-Gbps millimeter-wave WPAN systems," Proc. IEEE Global Telecommun. Conf. (GLOBECOM 2009), pp.1–6, Nov. 2009.
- [162] J. Wang et al., "Beam codebook based beamforming protocol for multi-Gbps millimeter-wave WPAN systems," IEEE J. Sel. Areas Commun., vol.27, pp.1390–1399, Oct. 2009.
- [163] S. Hur et al., "Millimeter wave beamforming for wireless backhaul and access in small cell networks," IEEE Trans. Wireless Commun., vol.61, pp.4391–4403, Oct. 2013.
- [164] M. Park, P. Gopalakrishnan, and R. Roberts, "Interference mitigation techniques in 60 GHz wireless networks," IEEE Commun. Mag., vol.47, no.12, pp.34–40, Dec. 2009.

- [165] M. Park and P. Gopalakrishnan, "Analysis on spatial reuse and interference in 60-GHz wireless networks," *IEEE J. Sel. Areas Commun.*, vol.27, pp.1443–1452, Oct. 2009.
- [166] U. Madhoo, "Networking at 60 GHz: The emergence of multigigabit wireless," *Proc. 2nd Int. Conf. Commun. Syst. Netw. (COMSNETS)*, pp.1–6, Jan. 2010.
- [167] C. Sheldon et al., "Four-channel spatial multiplexing over a millimeter-wave line-of-sight link," *Proc. 2009 MTT-S Int. Microw. Symp. Dig. (MTT '09)*, pp.389–392, June 2009.
- [168] E. Torkildson, U. Madhoo, and M. Rodwell, "Indoor millimeter wave MIMO: Feasibility and performance," *IEEE Trans. Wireless Commun.*, vol.10, pp.4150–4160, Dec. 2011.
- [169] K. Haneda, A. Khatun, C. Gustafson, and S. Wyne, "Spatial degrees-of-freedom of 60 GHz multiple-antenna channels," *Proc. IEEE 77th Veh. Technol. Conf. (VTC 2013-Spring)*, pp.1–5, June 2013.
- [170] K. Haneda et al., "Measurement-based analysis of spatial degrees of freedom in multipath propagation channels," *IEEE Trans. Antennas Propag.*, vol.61, no.2, pp.890–900, Feb. 2013.
- [171] J. Brady, N. Behdad, and A. Sayeed, "Beamspace MIMO for millimeter-wave communications: System architecture, modeling, analysis, and measurements," *IEEE Trans. Antennas Propag.*, vol.61, pp.3814–3827, July 2013.
- [172] A. Alkhateeb, O.E. Ayach, G. Leus, and R.W. Heath, Jr., "Channel estimation and hybrid precoding for millimeter wave cellular systems," *IEEE J. Sel. Top. Signal Process.*, vol.8, no.5, pp.831–846, Oct. 2014.
- [173] O. El Ayach et al., "Spatially sparse precoding in millimeter wave MIMO systems," *IEEE Trans. Wireless Commun.*, vol.13, no.3, pp.1499–1513, March 2014.
- [174] A. Alkhateeb, J. Mo, N. Gonzalez-Prelcic, and R.W. Heath, "MIMO precoding and combining solutions for millimeter-wave systems," *IEEE Commun. Mag.*, vol.52, no.12, pp.122–131, Dec. 2014.
- [175] S. Sun, T.S. Rappaport, R.W. Heath, A. Nix, and S. Rangan, "MIMO for millimeter-wave wireless communications: Beamforming, spatial multiplexing, or both?," *IEEE Commun. Mag.*, vol.52, no.12, pp.110–121, Dec. 2014.
- [176] A.A. Glazunov et al., "Spherical vector wave expansion of gaussian electromagnetic fields for antenna-channel interaction analysis," *IEEE Trans. Antennas Propag.*, vol.57, no.7, pp.2055–2067, July 2009.
- [177] J. Hansen, *Spherical near-field antenna measurement*, IEE Electromagnetic waves series 26, Peter Peregrinus, London, UK, 1998.
- [178] J.W. Wallace and M.A. Jensen, "Intrinsic capacity of the MIMO wireless channel," *Proc. IEEE 56th Veh. Technol. Conf. (VTC 2002-Fall)*, pp.701–705, 2002.
- [179] K. Haneda, C. Gustafson, and S. Wyne, "60 GHz spatial transmission: Multiplexing or beamforming?," *IEEE Trans. Antennas Propag.*, vol.61, pp.5735–5743, Nov. 2013.
- [180] Y.M. Tsang and A.S.Y. Poon, "Detecting human blockage and device movement in mmwave communication system," *Proc. IEEE Global Commun. Conf. (Globecom 2011)*, pp.1–6, Houston, TX, Dec. 2011.
- [181] M. Flament and M. Unbehaun, "Impact of shadow fading in a mm-wave band wireless network," *Proc. IEEE Int. Symp. Wireless Personal Multimedia Commun.*, 2000.
- [182] K. Sato and T. Manabe, "Estimation of propagation-path visibility for indoor wireless LAN systems under shadowing condition by human bodies," *Proc. 48th IEEE Veh. Technol. Conf. (VTC 1998)*, pp.2109–2113, May 1998.
- [183] J. Poutanen et al., "Multi-link MIMO channel modeling using geometry-based approach," *IEEE Trans. Antennas Propag.*, vol.60, no.2, pp.587–596, Feb. 2012.
- [184] A. Pellegrini et al., "Antennas and propagation for body-centric wireless communications at millimeter-wave frequencies: A review," *IEEE Antennas Propag. Mag.*, vol.55, no.4, pp.262–287, Aug. 2013.
- [185] S. Cotton, W. Scanlon, and B. Madahar, "Simulation of millimetre-wave channels for short-range body to body communications," *Proc. 4th European Conf. Antennas Propag. (EuCAP 2010)*, pp.1–5, April 2010.
- [186] J. Karedal et al., "A geometry-based stochastic MIMO model for vehicle-to-vehicle communications," *IEEE Trans. Wireless Commun.*, vol.8, no.7, pp.3646–3657, July 2009.
- [187] V. Nurmela and P. Kyosti, "A spatially consistent radio channel model enabling dual mobility," *Proc. IEEE 80th Veh. Technol. Conf. (VTC 2014-Fall)*, 4E-3, Vancouver, BC, Sept. 2014.
- [188] G. Allen and A. Hammoudeh, "Outdoor narrow band characterization of millimetre wave mobile radio signals," *Proc. IEE Colloq. Radiocomm. in the Range 30–60 GHz*, pp.4/1–4/7, Jan. 1991.
- [189] R. Davies, M. Bensebti, M. Beach, and J. McGeehan, "Wireless propagation measurements in indoor multipath environments at 1.7 GHz and 60 GHz for small cell systems," *Proc. 41st IEEE Veh. Technol. Conf. (VTC 1991)*, pp.589–593, May 1991.
- [190] H. Yang, P. Smulders, and M. Herben, "Indoor channel measurements and analysis in the frequency bands 2 GHz and 60 GHz," *Proc. IEEE 16th Int. Symp. Personal, Indoor and Mobile Radio Commun (PIMRC 2005)*, pp.579–583, Sept. 2005.
- [191] A. Plattner, N. Prediger, and W. Herzig, "Indoor and outdoor propagation measurements at 5 and 60 GHz for radio LAN application," *Proc. 1993 MTT-S Int. Microw. Symp. Dig.*, vol.2, pp.853–856, June 1993.
- [192] M. Peter and W. Keusgen, "Analysis and comparison of indoor wideband radio channels at 5 and 60 GHz," *Proc. 3rd European Conf. Antennas Propag. (EuCAP 2009)*, pp.3830–3834, March 2009.
- [193] H. Droste and G. Kadel, "Measurement and analysis of wide band indoor propagation characteristics at 17 GHz and 60 GHz," *Proc. 9th Int. Conf. Antennas Propag.*, pp.288–291, April 1995.
- [194] P. Nobles and F. Halsall, "Indoor propagation at 17 GHz and 60 GHz-measurements and modelling," *Proc. 1999 IEE Nat. Conf. Antennas Propag.*, pp.93–96, April 1999.
- [195] M. Schack, M. Jacob, and T. Kuerner, "Comparison of in-car UWB and 60 GHz channel measurements," *Proc. 4th European Conf. Antennas and Propag. (EuCAP)*, pp.1–5, April 2010.
- [196] M.T. Martinez-Ingles et al., "Experimental comparison between centimeter- and millimeter-wave ultrawideband radio channels," *Radio Sci.*, vol.49, no.6, pp.450–458, 2014.
- [197] M.T. Martinez-Ingles et al., "Experimental comparison of UWB against mm-wave indoor radio channel characterization," *Proc. 2013 IEEE Antennas Propag. Soc. Int. Symp. (APSURSI)*, pp.1946–1947, July 2013.
- [198] J. Poutanen et al., "Development of measurement-based ray tracer for multi-link double directional propagation parameters," *Proc. 3rd European Conf. Antennas Propag. (EuCAP 2009)*, pp.2622–2626, March 2009.
- [199] S. Hur et al., "Synchronous channel sounder using horn antenna and indoor measurements on 28 GHz," *Proc. IEEE Int. Black Sea Conf. Commun. Netw. (BlackSeaCom 2014)*, pp.83–87, Chisinau, Moldova, May 2014.



Katsuyuki Haneda received the Doctor of Engineering from the Tokyo Institute of Technology, Tokyo, Japan, in 2007. Having served as a post-doctoral researcher at the SMARAD Centre of Excellence in the Aalto University (former Helsinki University of Technology) School of Science and Technology, Dr. Haneda is presently an assistant professor in the Aalto University School of Electrical Engineering, Espoo, Finland. Dr. Haneda was the recipient of the best paper award of the antennas and propaga-

tion track in the IEEE 77th Vehicular Technology Conference (VTC2013-Spring), Dresden, Germany, and of the best propagation paper award in the 7th European Conference on Antennas and Propagation (EuCAP2013), Gothenburg, Sweden. Dr. Haneda has been serving as an associate editor for the IEEE Transactions on Antennas and Propagation since 2012 and as an editor for the Antennas, Channel Models, and Location Area of the IEEE Transactions on Wireless Communications since 2013. He also served as a co-chair of the topical working group on indoor environment in the European COST Action IC1004 Cooperative radio communications for green smart environments for two years during 2011–2013. His current research activity focuses on high-frequency radios such as millimeter-wave and beyond, wireless for medical scenario, radio wave propagation prediction, and in-band full-duplex radio technology.